

# Diffraction properties of volume phase gratings in photorefractive sillenite crystals of arbitrary cut under the influence of an external electric field

N. C. Deliolanis,\* I. M. Kourmoulis, A. G. Apostolidis, and E. D. Vanidhis

*Department of Physics, Aristotle University of Thessaloniki, Solid State Section 313-1, GR 541 24 Thessaloniki, Greece*

D. G. Papazoglou

*Foundation for Research and Technology–Hellas (FORTH), Institute of Electronic Structure & Laser, P.O. Box 1527, Vassilika Vouton, Heraklion GR 711 10, Crete, Greece*

(Received 1 April 2003; published 20 November 2003)

We study the influence of bias dc electric field on the optical properties of volume phase gratings formed in optically active photorefractive sillenite crystals. By considering a general case where the external electric bias direction, the grating vector orientation, the light propagation direction (crystal cut), and state of polarization are arbitrary, we deduce analytical expressions for the diffraction efficiency and the polarization state of the diffracted beam. The influence of the inverse piezoelectric effect is taken into account both in the uniform and the spatially varying part of the impermeability tensor, as well as into the calculation of the effective static permittivity. A theoretical comparative study of the dynamic behavior of the diffraction efficiency as a function of the physical parameters that affect the diffraction process (crystal cut, electric bias, input polarization, and grating orientation) along with experimental verification is provided. The general analytical solution provides means of exploitation of the capabilities of sillenite crystals in several applications.

DOI: 10.1103/PhysRevE.68.056602

PACS number(s): 42.40.Pa, 42.65.Hw, 42.70.Nq

## I. INTRODUCTION

The photorefractive crystals of the sillenite class 23 [ $\text{Bi}_{12}\text{SiO}_{20}$  (BSO),  $\text{Bi}_{12}\text{GeO}_{20}$  (BGO),  $\text{Bi}_{12}\text{TiO}_{20}$  (BTO)] have been widely studied (see Refs. [1,2] and references therein) and have been extensively used in optical signal processing and interferometric applications (see, for example, Refs. [3–8]). There are various characteristics and parameters that complicate the theoretical treatment of the diffraction from gratings recorded in sillenite crystals. The simultaneous appearance of the natural optical activity (which does not appear in other photorefractive materials), the electro-optic effect, as well as the secondary electro-optic effect (which is the combination of inverse piezoelectric and photoelastic effects) influences the propagation and the diffraction of both the transmitted and the diffracted beams. Another important parameter is the crystal configuration, which includes the orientation of the input and output faces of the crystal (the crystal cut), the grating vector orientation, and the external bias orientation. The bisectrix of the recording beams is perpendicular to the input face and determines the direction of propagation; the grating orientation determines the direction of the space charge field modulation and finally the external bias determines the bulk birefringence of the crystal. Consequently, diffraction is influenced by the configuration since both the primary and the secondary electro-optic effects depend on the orientation of space charge field and the external bias. Due to the theoretical complexity of light diffraction phenomena in optically active, photorefractive piezocrystals of the sillenite class, the

optimum operational conditions are not easy to find and a general analytical solution for the diffraction phenomena where the crystal configuration, the thickness, and state of polarization are arbitrary is necessary in order to optimize the parameter space. During the past years various papers have been published approaching the most general case by incorporating more parameters into the calculations.

In mid 1980s the first approaches treating these phenomena appeared. Analytical formulas for the intensity and the polarization properties of the diffracted beam for the usual configurations on  $(1\bar{1}0)$ -cut BSO crystals regarding optical activity have been provided by Shepelevich [9], and also including induced birefringence due to applied electric field by Marrakchi *et al.* [10] (numerical solution) and Mallick *et al.* [11] (analytical solution). Vachss *et al.* [12] and Pauliat *et al.* [13] presented solutions also for the off-Bragg anisotropic diffraction. Two-wave mixing was examined for the same configurations by Mallick *et al.* [14] and by Pauliat *et al.* [15]. Later on, Khramovich *et al.* [16,17] presented one of the first concise analytical solutions for light diffraction phenomena of transmission gratings arbitrarily oriented in the  $(110)$  crystallographic plane under the influence of an external electric field. The effect of the birefringence induced by the external field was also considered on studies of the evolution of the polarization of the diffracted beam [18,19].

Over those years, the importance of the piezoelectric effect on the diffraction phenomena became gradually evident. Izvanov *et al.* [20] calculated the influence of the secondary electro-optic effect on the photorefractivity of  $\text{LiNbO}_3$  and their theory was used by Stepanov *et al.* [21] to calculate the photoelastic contribution to the refractive index of a grating recorded in  $(110)$ -cut sillenites. The dependence of the components of the impermeability tensor on an inhomogeneous

\*Electronic address: optlab@auth.gr

space charge electric field with an arbitrarily oriented grating vector was presented by Shandarov *et al.* [22]. On the other hand, Günter and Zgonik [23] and Pauliat *et al.* [24] showed the influence of the inhomogeneous space charge electric field of an arbitrarily oriented grating on the static dielectric constant of a cubic crystal. The above results were included in the calculations of diffraction efficiency (DE) [25] and two-wave mixing (TWM) [26] of the (110)-cut for arbitrary grating orientation.

Recently, many studies regarding diffraction and two beam coupling in gratings recorded in (110) and (111)-cut sillenites have appeared including the optical activity and the piezoelectric effect. The optimization over several parameters (input polarization, grating vector orientation, crystal thickness) in the (110) cut was examined in Refs. [27–31], the recent (111)-cut was investigated in Refs. [32–37] and TWM under dc and ac electric field bias was considered in Refs. [38–41]. García *et al.* [42] have presented results on optimization with respect to the off-Bragg angle and electric field but ignoring optical activity.

The examined configurations in the above papers were either the (110) cut or the (111) cut. However, there is interest in examining the general case of arbitrary cut crystals with arbitrary grating vector orientation. Eichler *et al.* [43] have calculated the TWM gain of arbitrary cut crystals of the  $\bar{4}3m$  space group, only they are optically inactive. Montemezzani and Zgonik [44] have also presented analytical results on diffraction efficiency for arbitrary cut in general anisotropic media including off-Bragg mismatches but they also did not consider optical activity. Shepelevich [45] presented the first analytical solution for the DE and the effective gain of a transmission grating recorded in a cubic optically active photorefractive crystal of an arbitrary crystal cut, without taking into account the influence of an external bias electric field. A generalized and compact analytical approach of the photorefractive wave coupling in cubic crystals which took into account optical activity and birefringence induced from external bias was presented by Sturman *et al.* [46]. Those results were used by Kamenov *et al.* [47] to examine two-wave mixing in the general cut and compare it with the (111) cut indicating that the (110) cut is the most efficient for two-wave mixing. Until presently, no complete study regarding the influence of the external bias on the arbitrary-cut diffraction problem has been presented.

In this paper we deduce analytical expressions for the diffraction efficiency of volume phase gratings recorded in cubic photorefractive piezoelectric sillenite crystals under the influence of external bias electric field. In contrast to the majority of the literature where these diffraction problems are addressed by deriving and solving the coupled wave differential equations, we use the simpler, yet accurate, method of summing up the amplitude of the diffracted beams coming from elementary gratings slices along the crystal depth [11,14,48,49,34,31]. We consider a general case, where the grating vector orientation, the external bias direction, the light propagation direction, and state of the input polarization are arbitrary. First of all, the secondary electro-optic effect contribution and the principal refractive indices are analytically calculated for an arbitrary cut. Then, the diffraction

efficiency and diffracted light state of polarization are analytically and explicitly expressed by the material physical parameters (e.g., electro-optic, piezoelectric, and photoelastic parameters, optical activity), the geometric terms (grating vector orientation, bias electric field orientation, light propagation direction), the crystal thickness, and the state of polarization of the input beam. The calculations are performed under the assumptions of undepleted input beam, paraxial propagation direction, on-Bragg diffraction conditions, and for a constant prerecorded grating. The theoretical results are applied to the two distinct (110) and (111) cuts and experimental verification is provided. Finally, the diffraction efficiency for arbitrarily cut crystal is investigated when electric field is applied and the grating vector orientation is such that DE is maximum or independent from the input polarization.

## II. CALCULATION OF THE REFRACTIVE INDEX CHANGE

### A. Space charge field

Before proceeding to the calculation of the diffraction properties of the grating it is essential to calculate the space charge field, the impermeability tensor changes under constant and spatially modulated electric field, and the refractive index changes that are induced by the electric field. The electric field inside the crystal is derived from the modulation of the space charge density in the form of  $\mathbf{E}_{sc} = \mathbf{E}_{sc}^o \cos(\mathbf{G} \cdot \mathbf{r})$  and the constant part results from the externally applied electric field  $\mathbf{E}_o$ .

Apart from the usual influence on the electro-optic coefficient, the piezoelectric effect also modifies the static permittivity of grating due to the deformations taking place inside the crystal [23,24,50]. Introducing this influence to the Poisson equation ( $\nabla \cdot \mathbf{D} = \rho$ ) results in a modified formula for the calculation of the space charge field [51,31]

$$\mathbf{E}_{sc}^o = \frac{\Lambda \rho_{sc}^o}{2\pi} (\epsilon_{ij}^s l_i l_j + e_{ijk} l_i l_j \gamma_{ki} e_{pij} l_p l_i)^{-1}, \quad (1)$$

where  $\Lambda$  is the period of the grating,  $\rho_{sc}^o$  is the amplitude of the space charge density, and the parentheses is the effective static permittivity  $\epsilon^{\text{eff}}$  of the grating, consisting of the ordinary  $\epsilon^{\text{ord}}$  and the piezoelectric  $\epsilon^{\text{pz}}$  parts. Here,  $\epsilon_{ij}^s$  is the static permittivity tensor,  $e_{ijk}$  is the piezoelectric tensor,  $\gamma_{ki}$  is the inverse of the Christoffel tensor  $\Gamma_{ik} = C_{ijkl} l_j l_l$ ,  $C_{ijkl}$  is the elastic stiffness tensor,  $\{l_1, l_2, l_3\}$  are the projections of the unit vector  $\hat{\mathbf{l}}$  to crystallographic axes (see Fig. 1), and all indices range from 1 to 3.

In order to calculate the products in Eq. (1), we follow the reduction of indices for the 23 class after Nye [52]. The suffix notation of the 81-element elastic stiffness tensor  $C_{ijkl}$  is reduced to 36-element  $c_{mn}$ , and of the 27-element piezoelectric tensor  $e_{ijk}$  to the 18-element  $e_{mn}$ . The independent nonzero elements for a 23 class BGO crystal are  $\epsilon^s = \epsilon_{11}^s = \epsilon_{22}^s = 51.5\epsilon_o$ ,  $e = e_{14} = e_{25} = e_{36} = 0.98 \text{ C/m}^2$ ,  $c_1 = c_{11} = c_{22} = c_{33} = 12.84 \times 10^{10} \text{ N/m}^2$ ,  $c_2 = c_{12} = c_{21} = c_{23} = c_{32} = c_{13} = c_{31} = 2.94 \times 10^{10} \text{ N/m}^2$ , and  $c_3 = c_{44} = c_{55} = c_{66}$

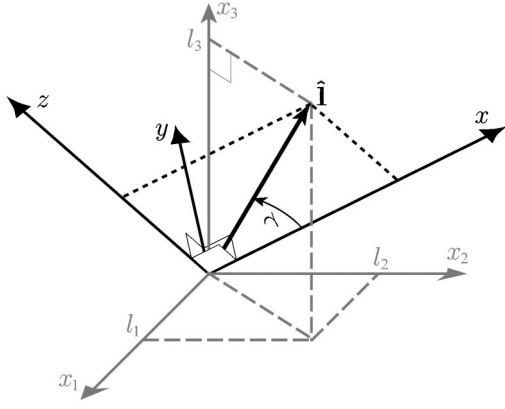


FIG. 1. Crystallographic  $\{Ox_1, Ox_2, Ox_3\}$  and laboratory  $\{Ox, Oy, Oz\}$  coordinate axes.  $Oy$  is the direction of light propagation and the  $\{Ox, Oz\}$  plane defines the front face of the crystal. Here,  $l_1$ ,  $l_2$ , and  $l_3$  are the projections of the unit vector  $\hat{\mathbf{I}}$  onto the crystallographic axes.

$= 2.55 \times 10^{10} \text{ N/m}^2$  [53]. After these replacements, we calculate the effective static permittivity tensor for arbitrary direction of the grating vector:

$$\epsilon^{\text{eff}} = \epsilon^{\text{ord}} + \epsilon^{\text{pz}} = \epsilon^s + \frac{4e^2}{A_4} (A_1 l_2^2 l_3^2 + A_2 l_3^2 l_1^2 + A_3 l_1^2 l_2^2), \quad (2)$$

where  $A_1$ ,  $A_2$ ,  $A_3$ , and  $A_4$  are

$$A_i = c_1 c_3 - c_3 (c_1 + c_3 + 2c_2) l_i^2 + (c_1 - c_2 - 2c_3) [(c_1 + c_2) l_j^2 l_k^2 - (c_2 + c_3) l_i^2 (1 - l_i^2)], \quad (3a)$$

$$A_4 = [(c_1 - c_3)(c_1 + c_2) - 2(c_2 + c_3)^2] l_1^2 l_2^2 l_3^2 (c_1 - c_2 - 2c_3) + c_1 c_3^2 + c_3 (c_1 + c_2) (l_1^2 l_2^2 + l_1^2 l_3^2 + l_2^2 l_3^2), \quad (3b)$$

where  $\{i, j, k\}$  in  $A_i$  are cyclic permutations of  $\{1, 2, 3\}$ .

The plot of the  $\epsilon^{\text{pz}}/\epsilon^{\text{ord}}$  ratio for arbitrary grating vector direction is shown in Fig. 2. The depicted surface is exhibiting the fourfold symmetry axes along the crystallographic axes, threefold along the  $\langle 111 \rangle$  and equivalent directions, and twofold along  $\langle 110 \rangle$  and equivalent which are including the expected symmetry elements of class 23. The influence of the piezoelectric effect is maximum (10.6% of  $\epsilon^{\text{ord}}$ ) when  $\mathbf{G}$  is along the  $\langle 110 \rangle$  directions, is zero when  $\mathbf{G}$  is along the principal crystallographic axes, and local minima (3.7% of  $\epsilon^{\text{ord}}$ ) are appearing when  $\mathbf{G}$  is parallel to  $\langle 111 \rangle$  directions. Consequently,  $E_{\text{sc}}^o$  is reduced down to 92.3% at  $\langle 110 \rangle$  and 97.2% at  $\langle 111 \rangle$  from its original value.

For the gratings recorded in Sec. V we assume that the amplitude of the space charge field  $\mathbf{E}_{\text{sc}}$  is proportional to externally applied electric field  $\mathbf{E}_o$ . When the grating forms an angle  $\gamma_G$  with the direction of the applied field, the component of  $\mathbf{E}_o$  contributing to the space charge buildup is proportional to  $\cos(\gamma_G)$ , or  $E_{\text{sc}}^o = \alpha \cos(\gamma_G) E_o \epsilon^s / \epsilon^{\text{eff}}$  [2,49,46], where  $\alpha$  is simply a scaling parameter indicating the efficiency of the space charge buildup.

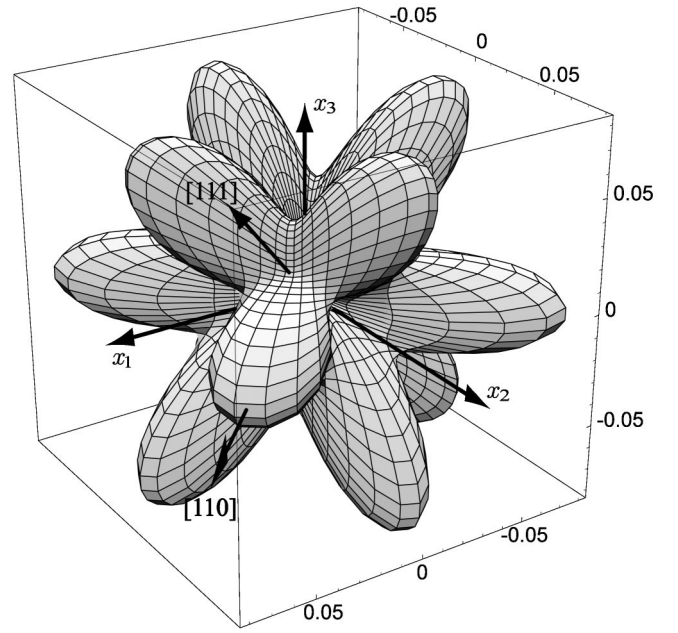


FIG. 2. Spherical plot of the  $\epsilon^{\text{pz}}/\epsilon^{\text{ord}}$  ratio for arbitrary grating vector direction for a BGO crystal.

## B. Refractive index change

The changes in the impermeability tensor  $[B_{ij} = (1/\epsilon_o) \epsilon_{ij}^{-1}]$  are attributed to the electro-optic and to the elasto-optic effect. For a homogenous electric field in an unclumped crystal there is homogenous deformation and the change in the impermeability tensor is

$$\Delta B_{mn}^o = E_o r_{mnp} l_p + E_o p_{mnkl} e_{pij} C_{klj}^{-1} l_p. \quad (4)$$

For a spatially modulated space charge field the amplitude of the impermeability tensor modulation is:

$$\Delta B_{mn}^{\text{sc}} = E_{\text{sc}}^o r_{mnp} l_p + E_{\text{sc}}^o p_{mnkl} \gamma_{ki} l_l e_{pij} l_p l_j, \quad (5)$$

where  $r_{mnp}$  is the electro-optic tensor and  $p_{mnkl}$  is the elasto-optic tensor. For  $\Delta B_{mn}^o$  in Eq. (4),  $l_1$ ,  $l_2$ , and  $l_3$  are the projections of  $\mathbf{E}_o/E_o$  to the crystallographic axes, while for  $\Delta B_{mn}^{\text{sc}}$  in Eq. (5) they are the projections of  $\mathbf{G}/G$ , which are generally not parallel. The 27-element electro-optic tensor is contracted down to 18-element  $r_{ij}$  and the 81-element elasto-optic tensor down to the 36-element  $p_{ik}$ . The independent nonzero elements for a BGO crystal are  $r = r_{41} = r_{52} = r_{63} = 3.14 \text{ pm/V}$  ( $\lambda = 645 \text{ nm}$ ) [54],  $p_1 = p_{11} = p_{22} = p_{33} = 0.12$ ,  $p_2 = p_{12} = p_{31} = p_{23}$ ,  $p_3 = p_{13} = p_{21} = p_{32}$ ,  $p_2 + p_3 = 0.19$ , and  $p_4 = p_{44} = p_{55} = p_{66} = 0.01$  [55]. We carry out the multiplications in Eqs. (4) and (5) and the on and off diagonal elements of the impermeability tensor for arbitrary direction of  $\mathbf{E}_o$  and  $\mathbf{G}$  become

$$\Delta B_{mm}^o = 0, \quad \Delta B_{mn}^o (m \neq n) = E_o (r + ep_4/c_3) l_p, \quad (6)$$

$$\Delta B_{mm}^{sc} = 2E_{sc}^o e l_m l_n l_p \frac{p_1 A_m + p_2 A_n + p_3 A_p}{A_4}, \quad (7)$$

$$\Delta B_{mn}^{sc} (m \neq n) = E_{sc}^o l_p \left( r + 2ep_4 \frac{A_n l_m^2 + A_m l_n^2}{A_4} \right),$$

where  $\{m, n, p\}$  are cyclic permutations of  $\{1, 2, 3\}$ , any recurrence of an index in these equations does not denote summation over this index, and  $A_1, A_2, A_3$ , and  $A_4$  are given from Eqs. (3).

The refraction indices of the eigenpolarizations are given by the length of the principal axes  $\{Ox', Oz'\}$  of the ellipse which is formed by the cross section of the indicatrix  $B_{ij} x_i x_j = 1$  with the plane which is perpendicular to the direction of propagation [52]. After some simple calculations we find that the changes of the refractive indices for an arbitrary cut sillenite crystal are

$$\Delta n_x = -\frac{1}{4} n_o^3 (Q_{11} + Q_{22} + Q_o),$$

$$\Delta n_z = -\frac{1}{4} n_o^3 (Q_{11} + Q_{22} - Q_o), \quad (8)$$

$$\tan(2\psi) = \frac{Q_{12} + Q_{21}}{Q_{11} - Q_{22}}, \quad \cos(2\psi) = \frac{Q_{11} - Q_{22}}{Q_o}, \quad (9)$$

where  $\psi$  is the angle between the  $Ox$  axis and the principal axis  $Ox'$ ,  $Q_{ij}$  and  $Q_o$  are

$$Q_{ij} = l_{mi} l_{nj} \Delta B_{mn},$$

$$Q_o = \sqrt{(Q_{11} - Q_{22})^2 + (Q_{12} + Q_{21})^2}. \quad (10)$$

Here,  $\{m, n\} = \{1, 2, 3\}$ ,  $\{i, j\} = \{x, z\}$ , and  $l_{mi}$  is the projection of  $l_m$  to  $i$  axis. The formulas for the calculation of  $\Delta n_x$  and  $\Delta n_z$  apply for both electric fields  $\mathbf{E}_o$  and  $\mathbf{E}_{sc}$ , the refractive indices are  $\Delta n_{x, z_{sc}}$  and  $\Delta n_{x, z_o}$ , the principal axes are  $\{Ox_o, Oz_o\}$  and  $\{Ox_{sc}, Oz_{sc}\}$ , and their orientations are  $\psi_o$  and  $\psi_{sc}$ , respectively (Fig. 5). Finally, the orientation of the principal axes depends only on the orientation of the electric field and not on its value.

### III. DIFFRACTION THEORY: THE ELEMENTARY SLICE APPROACH

In the case of a birefringent and optically active crystal the process of diffraction from volume phase gratings involves two phenomena, the propagation of light in the crystal and diffraction itself, and they are described by the general two-wave mixing equation in tensorial form

$$\nabla^2 \mathbf{E} - \nabla(\nabla \cdot \mathbf{E}) + \omega^2 \mu [\epsilon_{ij}^o + \delta \epsilon_{ij}^{sc} \cos(\mathbf{G} \cdot \mathbf{r})] \mathbf{E} = \mathbf{0}, \quad (11)$$

where  $\mathbf{E}$  is the optical electric field,  $\mathbf{G}$  is the grating vector, and  $\mu$  is the magnetic permeability. The electric permittivity

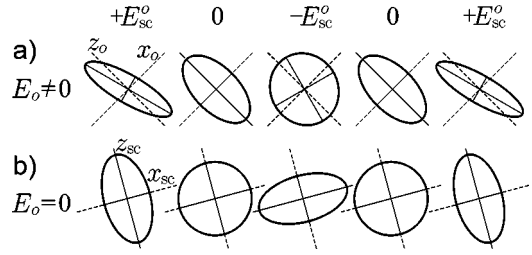


FIG. 3. Various phases of the indicatrix section along a grating period (not in scale). (a) When electric bias field is applied ( $\mathbf{E}_o \neq 0$ ) the indicatrix has a mean orientation  $\{Ox_o, Oz_o\}$  and ellipticity. Under the influence of the space charge field ( $\mathbf{E}_{sc}$  is generally not parallel to  $\mathbf{E}_o$ ) the section is tilted and its ellipticity is modulated around the mean value. (b) When  $\epsilon_{ij}^o$  is isotropic ( $\mathbf{E}_o = 0$ , or for an elementary grating) the indicatrix is influenced by  $\delta \epsilon_{ij}^{sc} \cos(\mathbf{G} \cdot \mathbf{r})$  alone, and the section has fixed orientation axes  $\{Ox_{sc}, Oz_{sc}\}$ .

is split into a constant bulk component  $\epsilon_{ij}^o$  and a spatially modulated component  $\delta \epsilon_{ij}^{sc} \cos(\mathbf{G} \cdot \mathbf{r})$  which are depending on the external bias and the space charge field, respectively. The simultaneous influence of the constant and the spatially modulated parts of the permittivity tensor throughout the entire crystal bulk leads to a nontrivial cross section pattern of the indicatrix [see Fig. 3(a)]. However, these two aspects can be treated independently by splitting the tensorial Eq. (11) into two eigenvector equations and then by following the analysis introduced by Mallick *et al.* [11].

We consider small elementary thin slices inside the crystal (Fig. 4) that are perpendicular to the general propagation direction (paraxial approximation) and that the electric field is perpendicular to the direction of propagation ( $\mathbf{E} \perp Oy$ ). If the permittivity tensor is expressed in the laboratory coordinate system  $\{Ox, Oy, Oz\}$ , then the eigenwave equations for the bulk and the modulated permittivity tensor are

$$\delta \epsilon_{ij}^{sc} \mathbf{E}_k^g = \delta \epsilon_k \mathbf{E}_k^g, \quad \epsilon_{ij}^o \mathbf{E}_l^b = \epsilon_l^o \mathbf{E}_l^b, \quad (12)$$

where  $\mathbf{E}_k^g$  and  $\mathbf{E}_l^b$  are the two eigenpolarization vectors of the spatially modulated ( $g$  grating) and the constant ( $b$  bulk) components of the reduced permittivity tensor as expressed in the lab coordinate system and  $\delta \epsilon_k$  and  $\epsilon_l^o$  are the eigenvalues, where  $i, j, k, l = \{1, 2\}$  (in this particular case the repeated indices  $k$  and  $l$  at the eigenvalue products  $\delta \epsilon_k \mathbf{E}_k^g$  and  $\delta \epsilon_l \mathbf{E}_l^g$  do not imply summing over the range of the indices). We can generally express an arbitrary light electric field vector  $\mathbf{E}$  as a linear combination of any of the eigenstate pairs:

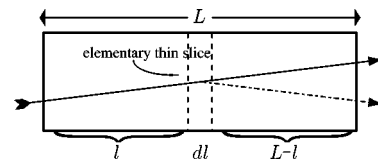


FIG. 4. Diffraction from an elementary thin slice  $dl$ .

$$\mathbf{E} = g_k(y)\mathbf{E}_k^g = b_l(y)\mathbf{E}_l^b, \quad (13)$$

where  $g_k(y)$  and  $b_l(y)$  are generally functions of crystal depth  $y$  that contain phase shift information due to propagation. The bulk eigenstates  $\mathbf{E}_l^b$  can also be expressed as a linear combination of the  $\mathbf{E}_k^g$  eigenstates

$$\mathbf{E}_l^b = d_{lk}\mathbf{E}_k^g. \quad (14)$$

By consecutively substituting Eqs. (13), (12), and (14) into Eq. (11), assuming an isotropic Bragg diffraction, and assuming that the coefficients  $g_k(y)$  and  $b_l(y)$  remain constant for an elementary thin slice of the crystal  $dl$  so that  $\nabla^2 g_k \mathbf{E}_k^g = g_k \nabla^2 \mathbf{E}_k^g$  and  $\nabla(\nabla \cdot g_k \mathbf{E}_k^g) = g_k \nabla(\nabla \cdot \mathbf{E}_k^g)$ , the two-wave mixing equation can be split into two scalar equations corresponding to the two eigenstates  $\mathbf{E}_k^g$ :

$$\nabla^2 \mathbf{E}_k^g - \nabla(\nabla \cdot \mathbf{E}_k^g) + \omega^2 \mu [\epsilon_k^{\text{sb}} + \delta \epsilon_k \cos(\mathbf{G} \cdot \mathbf{r})] \mathbf{E}_k^g = \mathbf{0}, \quad (15)$$

where  $\epsilon_k^{\text{sb}} = \epsilon_l^o b_l d_{lk} / (b_l d_{lk})$  are the scalar bulk permittivities. The value of each scalar bulk permittivity  $\epsilon_k^{\text{sb}}$  oscillates between the two bulk eigenvalues  $\epsilon_l^o$  of the permittivity tensor  $\epsilon_{ij}^o$  and it depends on the polarization of the input beam.

It is clear that the problem of light propagation and diffraction through an elementary periodic grating slice can be simplified to two eigenvector TWM equations with the use of the eigenvectors of the grating  $\mathbf{E}_k^g$ . Considering that electrogyration is negligible in sillenites, the eigenvectors of the grating are linearly polarized (see Sec. II B) and the problem is simplified. The solution of the scalar diffraction problem is well known by Kogelnik [56] and the amplitude of the diffracted beam is

$$\mathbf{U}_k = -i \sin \frac{\pi \delta \epsilon_k L}{2 \epsilon_k^{\text{sb}} \lambda_m \cos \theta_B} \mathbf{E}_k^g = -i \sin \frac{\pi \Delta n_k L}{\lambda \cos \theta_B} \mathbf{E}_k^g, \quad (16)$$

where  $\lambda_m$  and  $\lambda$  are, respectively, the wavelengths in the medium and in vacuo,  $\theta_B$  is the Bragg angle, and  $L$  is the crystal thickness. Here,  $\Delta n_k$  are amplitudes of the refractive index modulation of the  $k = \{x_{\text{sc}}, z_{\text{sc}}\}$  eigenstates that were calculated in Eq. (8) and are illustrated in Fig. 3(b). For the paraxial approximation, it is  $\cos \theta_B \approx 1$  and the resulting diffracted beam has the same polarization as the input eigenpolarization. If we assume that the diffraction efficiency is low so that the portion of diffracted light that diffracts back to the original direction is negligible, the amplitude of the light electric field eigenvector that is diffracted from an elementary slice  $dl$  of the grating is

$$d\mathbf{U}_k \approx -i \frac{\pi \Delta n_k dl}{\lambda} \mathbf{E}_k^g. \quad (17)$$

The total light electric field of the diffracted beam at the exit of the crystal is the sum of the elementary electric fields of the diffracted beams from each elementary slice and it can be calculated by integrating  $d\mathbf{U}_k$  over the entire crystal depth. However, the polarization of light is changing when propagating through crystal depth due to the bulk birefrin-

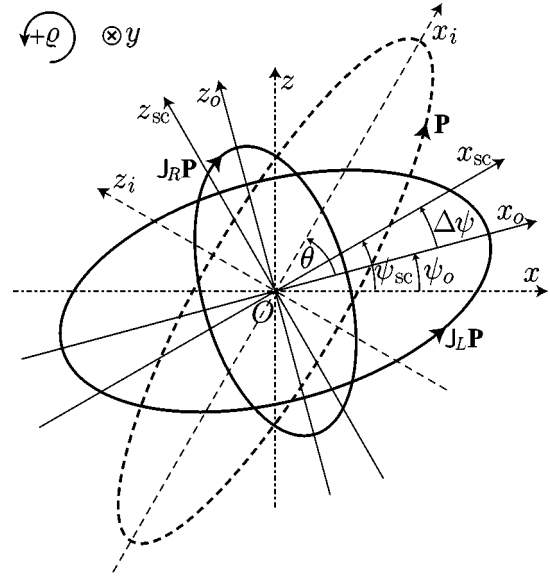


FIG. 5. Analysis of the input  $\mathbf{P}$  into the two eigenpolarization states  $\mathbf{J}_L \mathbf{P}$  and  $\mathbf{J}_R \mathbf{P}$ .  $\{Ox, Oz\}$ ,  $\{Ox_i, Oz_i\}$ ,  $\{Ox_o, Oz_o\}$ , and  $\{Ox_{\text{sc}}, Oz_{\text{sc}}\}$  are the external, the input, the bulk eigenstate and the grating eigenstate, coordinate systems. The positive sense of rotation is indicated.

gence and optical activity. Although these phenomena are neglected while light is diffracted by the elementary grating, they should be taken into consideration both before and after the diffraction. This means that the light entering the crystal should be analyzed into the bulk eigenstates  $\mathbf{E}_l^b$  which propagate independently with different velocity until the grating. Then they are analyzed into the grating eigenstates  $\mathbf{E}_k^g$ , they are diffracted, and the diffracted beams are analyzed again back to  $\mathbf{E}_l^b$  eigenstates which propagate independently in the same manner until the exit of the crystal. In this way the diffracted light beam which comes from the grating contains the information of bulk polarization. Integrating over the crystal depth results in the total electric field of the diffracted beam; the process of integration combines both diffraction and propagation phenomena.

#### IV. OUTLINE OF THE PROCEDURE FOLLOWED TO CALCULATE THE DIFFRACTION PROPERTIES

We shall follow the Jones calculus notation to describe the calculation of the diffracted beam amplitude. We consider that the light entering the front face of the crystal is generally elliptically polarized,  $\mathbf{P}_i$  is the vector of the electric field, and  $P_o^2$  is its intensity. Assuming a paraxial direction of propagation so that the light electric field does not have components on  $Oy$  axis, the polarized light expressed in matrix notation on the  $Ox_i, Oz_i$  axes is

$$\mathbf{P}_i = \frac{1}{\sqrt{1 + \epsilon^2}} P_o e^{-i\omega t} \begin{pmatrix} 1 \\ i\epsilon \end{pmatrix}_i, \quad (18)$$

where  $\epsilon$  is its ellipticity defined as the ratio of the  $z_i$  to the  $x_i$  axes of the ellipse ( $\epsilon \in \Re$ ) (see Fig. 5). If  $\epsilon = 0$ , the light is

linearly polarized, and if  $\varepsilon \geq 0$ , the sense of rotation is anticlockwise or clockwise, respectively, for an observer who is looking along the direction of the propagation of light—the convention that the anticlockwise rotation along the direction of propagation is positive is to be followed throughout the paper. The small index at the lower right corner of the matrix denotes the set of axes that the components of the vector refer to, e.g.,  $i$  indicates the  $Ox_i, Oz_i$  axes. The two components of the elliptically polarized light  $\mathbf{P}_i$  are projected to the eigenaxes  $Ox_o, Oz_o$  by multiplying with the rotation matrix  $\mathbf{R}(\theta) = \begin{pmatrix} \cos \theta & \sin \theta \\ \sin \theta & \cos \theta \end{pmatrix}$  and the resulting light electric field at the entrance face ( $l=0$ ) is

$$\mathbf{P}_o(0) = \mathbf{R}(-\theta)\mathbf{P}_i. \quad (19)$$

$\mathbf{P}_o(0)$  can be analyzed into the two elliptical eigenstates of polarization by multiplying with the eigenstate matrices  $\mathbf{J}_L$  and  $\mathbf{J}_R$  given by the equations

$$\mathbf{J}_L = \frac{1}{1+k^2} \begin{pmatrix} 1 & -ik \\ ik & k^2 \end{pmatrix}, \quad \mathbf{J}_R = \frac{1}{1+k^2} \begin{pmatrix} k^2 & ik \\ -ik & 1 \end{pmatrix}, \quad (20)$$

where  $k$  is the ellipticity ( $|k| \leq 1$ ) of the elliptic eigenpolarizations. According to Nye [52] the ellipticity  $k$  of the eigenstates of polarization is

$$k = \tan \left[ \frac{1}{2} \arctan \left( \frac{2\varrho}{\delta} \right) \right], \quad (21)$$

where  $\delta$  is the phase difference per unit length between the two eigenpolarizations regarding the birefringence alone and  $\varrho$  is the rotation of the polarization plane per unit length regarding optical activity alone. The phase difference  $\delta$  is calculated from the refraction indices along the  $Ox_o, Oz_o$  axes

$$\delta = \frac{2\pi}{\lambda} (\Delta n_{z_o} - \Delta n_{x_o}). \quad (22)$$

The total phase difference between the two elliptic eigenpolarizations is connected with the phase difference  $\delta$  and the rotatory power  $\varrho_o$ ,

$$\phi^2 = \delta^2 + (2\varrho)^2. \quad (23)$$

After propagating to crystal depth  $l$ , the “fast” eigenstate gains a phase difference  $\phi l$  over the “slow” and light electric field turns out to be

$$\mathbf{P}_o(l) = e^{-i\phi l} \mathbf{J}_L \mathbf{P}_o(0) + \mathbf{J}_R \mathbf{P}_o(0). \quad (24)$$

In order to calculate the portion of the light that is diffracted from the elementary slice  $dl$ , the components of  $\mathbf{P}_o(l)$  must be rotated to the  $Ox_{sc}, Oz_{sc}$  principal axes of the

section of index ellipsoid of the periodic phase grating (also named diffracting axes) which are lying at an angle  $\Delta\psi$  to  $Ox_o$ . The elementary diffracted components are parallel to their diffracting axes and according to the approach described in Sec. III [Eq. (17)] the Jones matrix of the diffracting grating slice is

$$\Delta n_{sc} = -i \frac{\pi dl}{\lambda} \begin{pmatrix} \Delta n_{x_{sc}} & 0 \\ 0 & \Delta n_{z_{sc}} \end{pmatrix}_{sc}. \quad (25)$$

Finally, the light electric field of the beam which is diffracted from the  $dl$  slice along the  $\{Ox_o, Oz_o\}$  axes is

$$d\mathbf{U}_o(l) = \mathbf{R}(-\Delta\psi) \Delta n_{sc} \mathbf{R}(\Delta\psi) \mathbf{P}_o(l). \quad (26)$$

The diffracted portion is analyzed into the two eigenstates of polarization which propagate independently till the back face of the crystal and a  $\phi(L-l)$  phase difference is introduced to the “fast” eigenstate:

$$d\mathbf{U}_o(L) = e^{-i\phi(L-l)} \mathbf{J}_L d\mathbf{U}_o(l) + \mathbf{J}_R d\mathbf{U}_o(l). \quad (27)$$

The output light electric field is calculated by integrating the elementary portions from the thin slices throughout the crystal depth:

$$\begin{aligned} \mathbf{U}_o(L) &= \int_{l=0}^L d\mathbf{U}_o(L) \\ &= \left[ L e^{-i\phi L} \mathbf{J}_L \mathbf{R}(-\Delta\psi) \Delta n_{sc} \mathbf{R}(\Delta\psi) \mathbf{J}_L \right. \\ &\quad + \frac{i}{\phi} (e^{-i\phi L} - 1) \mathbf{J}_L \mathbf{R}(-\Delta\psi) \Delta n_{sc} \mathbf{R}(\Delta\psi) \mathbf{J}_R \\ &\quad + \frac{i}{\phi} (e^{-i\phi L} - 1) \mathbf{J}_R \mathbf{R}(-\Delta\psi) \Delta n_{sc} \mathbf{R}(\Delta\psi) \mathbf{J}_L \\ &\quad \left. + L \mathbf{J}_R \mathbf{R}(-\Delta\psi) \Delta n_{sc} \mathbf{R}(\Delta\psi) \mathbf{J}_R \right] \mathbf{P}_o(0). \quad (28) \end{aligned}$$

The above equation is actually the transfer function of Bragg diffraction from the volume phase grating, and it consists of two intramodal diffraction components (diffraction to the same eigenmode) and of two intermodal components (diffraction to the opposite eigenmode). The terms inside the brackets constitute the  $2 \times 2$  Jones matrix of the diffraction grating. We calculate  $\mathbf{U}_o(L)$  in analytical form by substituting Eqs. (18), (19), (20), and (25) into Eq. (28),

$$\mathbf{U}_o(L) = e^{-i\omega t} \begin{pmatrix} A + iB \\ C + iD \end{pmatrix}_o, \quad (29)$$

where  $\{A, B, C, D\} \in \mathfrak{R}$  are defined in the Appendix, see Eq. (A1). The diffraction efficiency  $\eta$  is the ratio of the diffracted to the input light intensity, that is,

$$\eta = \frac{\left\langle \frac{1}{2} \mathbf{U}_o(L) \cdot \mathbf{U}_o(L)^* \right\rangle}{\left\langle \frac{1}{2} \mathbf{P}_o(0) \cdot \mathbf{P}_o(0)^* \right\rangle} = \frac{A^2 + B^2 + C^2 + D^2}{P_o^2}. \quad (30)$$

After a few calculations an analytical formula for diffraction efficiency with the following format can be found:

$$\eta = \eta_{dc} + \eta_{ac_1} \cos(2\theta) + \eta_{ac_2} \sin(2\theta) = \eta_{dc} + \eta_{ac} \cos(2\theta + \xi), \quad (31)$$

where

$$\eta_{ac} = \sqrt{\eta_{ac_1}^2 + \eta_{ac_2}^2}, \quad (31a)$$

$$\xi = -\arctan \frac{\eta_{ac_2}}{\eta_{ac_1}} + \begin{cases} \pi & \text{if } \eta_{ac_1} \leq 0 \\ 0 & \text{if } \eta_{ac_1} > 0, \end{cases} \quad (31b)$$

where  $\eta_{dc}$ ,  $\eta_{ac_1}$ ,  $\eta_{ac_2}$  are presented in the Appendix:

The azimuth  $\psi_{az}$ , the ellipticity  $\varepsilon_o$ , and the sense of rotation  $s$  of the diffracted light can be determined from Eq. (28). After some simple calculations the derived formulas are

$$\tan(2\psi_{az}) = \frac{2(AC+BD)}{A^2+B^2-C^2-D^2} = \frac{p}{q}, \quad (32a)$$

$$\varepsilon_o^2 = \frac{A^2+B^2+C^2+D^2 - \sqrt{4(AC+BD)^2 + (A^2+B^2-C^2-D^2)^2}}{A^2+B^2+C^2+D^2 + \sqrt{4(AC+BD)^2 + (A^2+B^2-C^2-D^2)^2}} = \frac{\eta P_o^2 - \sqrt{p^2+q^2}}{\eta P_o^2 + \sqrt{p^2+q^2}}, \quad (32b)$$

$$s = \begin{cases} \text{anticlockwise} & \text{if } AD - BC > 0 \\ \text{linearly polarized} & \text{if } AD - BC = 0 \\ \text{clockwise} & \text{if } AD - BC < 0. \end{cases} \quad (32c)$$

When no electric field is applied ( $E_o = 0$ ) and for linearly polarized input  $\varepsilon = 0$  [34],  $\eta_{dc}$ ,  $\eta_{ac}$ , and  $\xi$  in Eqs. (A2) are reduced to

$$\eta_{dc} = \frac{\pi^2 L^2}{4\lambda^2} [(\Delta n_{x_{sc}} - \Delta n_{z_{sc}})^2 \text{sinc}^2(\varrho L) + (\Delta n_{x_{sc}} + \Delta n_{z_{sc}})^2], \quad (33a)$$

$$\eta_{ac} = \frac{\pi^2 L^2}{2\lambda^2} (\Delta n_{x_{sc}}^2 - \Delta n_{z_{sc}}^2) \text{sinc}(\varrho L), \quad (33b)$$

$$\xi = \varrho L - 2\psi_{sc}. \quad (33c)$$

Additionally, the theoretical results are in agreement with the analysis on the  $(1\bar{1}0)$  cut in Ref. [11] and also with the results on DE versus  $E_o$  and thickness in Ref. [46].

## V. EXPERIMENT AND COMPARISON WITH THEORY

### A. Experimental procedure

In this section measurements of the intensity (diffraction efficiency) and the polarization state (azimuth and ellipticity) of the beam that is diffracted from gratings recorded in BGO crystal are presented. In order to examine every aspect of the theory, the variable parameters of the experiments are the grating vector orientation, the input polarization, and the strength of the externally applied electric field during read-out.

The experimental setup for two-wave mixing experiments is depicted in Fig. 6. A collimated beam, produced from

Hg-Xe white arc lamp, the wavelength of which is selected by an interference filter, illuminates the grating. The image of the grating is formed on the crystal with the use of two lenses  $L_1$  and  $L_2$ , as shown in Fig. 6. By placing two apertures in the Fourier plane between the lenses, transmission is allowed only for the  $\pm 1$  diffracted orders, so that the filtered image which is projected to the crystal has sinusoidal profile with period  $\Lambda = 25 \mu\text{m}$  (far drift region). The grating is recorded using 545 nm unpolarized light, the modulation is  $m = 1$ , and the total exposure is  $0.4 \text{ mJ/cm}^2$ ; during the recording a static electric field is externally applied. For the readout process 645 nm illumination is selected, the  $a_{-1}$  aperture is blocked so that only one diffraction order is transmitted to the crystal, and the diffracted light is gathered into a photomultiplier (PM). For the measurement of the DE of the grating, a polarizer is placed before the crystal and dividing the intensity of the diffracted to the transmitted beam yields the DE. For each particular grating  $\eta_{ac}$  and  $\eta_{dc}$  are measured by rotating the polarizer and calculating the amplitude and the mean value of the signal, respectively. For the measurement of the polarization state of the diffracted beam a rotating analyzer is placed behind the crystal.

In our experiments it was noticed that the effective values of the electric field that best fitted the experimental results were about 40–50% lower than the externally applied field which was calculated from the applied voltage  $V/d$ . This deviation is attributed to an inverse static electric field that is building up during recording, which is reducing the strength of the originally applied electric field and which is probably inhomogeneous. The buildup of this screening field was noticed in various experiments [12,18,57–62] and is attributed

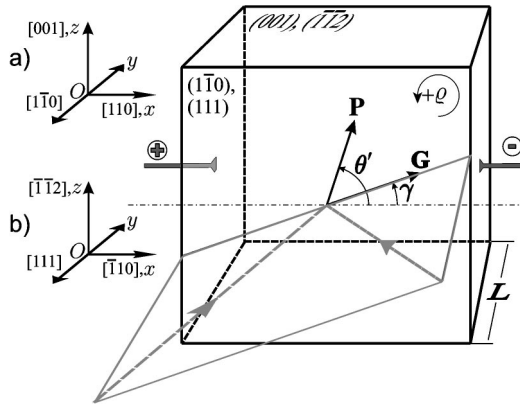


FIG. 7. Crystal configuration (a) the  $(1\bar{1}0)$  cut and (b)  $(111)$  cut. Here,  $\theta'$  and  $\gamma_G$  are measured from the  $Ox$  axis.

to the resistance of the contacts and to the inhomogeneous illumination of the crystal. In order to verify this hypothesis we measured the polarization state of a beam that is directly transmitted (not diffracted) through the grating and taking under consideration the effects of optical activity and induced birefringence. The results showed the existence of this inverse field and its effective value explained the “loss” that was noticed in the first place. The existence of the screening field can be an advantage in DE and polarization measurements. In order to achieve higher electric fields inside the crystal we switch the polarity of the applied voltage during readout so that the screening field that has been build up during recording is now added rather than subtracted.

### B. Results for the $(1\bar{1}0)$ and $(111)$ cuts

The two distinct cuts on photorefractive sillenite crystals are along the  $(110)$  and equivalent planes, which is also known as the Huigniard configuration, and along  $(111)$  and equivalent planes. In our experiments a 5.5 mm thick  $(1\bar{1}0)$ -cut positive ( $\varrho > 0$ ) BGO and a 5 mm  $(111)$ -cut negative ( $\varrho < 0$ ) BGO are used according to the configuration shown in Fig. 7.

First we examine the DE of the  $(1\bar{1}0)$ -cut BGO when the external bias field is applied along  $[110]$ . A grating is recorded using an  $E_o = +8$  kV/cm external bias and during readout (a) an opposite bias ( $E_o = -8$  kV/cm) and (b) no bias ( $E_o = 0$  kV/cm) are applied. The experimental and the theoretical results of DE versus grating vector orientation are depicted in Figs. 8(a) and 8(b). DE consists of the mean part  $\eta_{dc}$  and the oscillating part whose amplitude is  $\eta_{ac}$  [see Eq. (31)] and has two lobes. DE is zeroed when the grating is recorded along  $[001]$  ( $\gamma = \pm 90^\circ$ ) because the component of

the external bias field along the grating is zero. It can be seen that when external field is applied during readout,  $\eta_{dc}$  is symmetric about  $\gamma = 0$  and it generally increases by about 50%, while for the (b) case the “right”  $\eta_{ac}$  lobe at  $\gamma > 0$  is lower compared to the  $\gamma < 0$  one. The optimum polarization angle ( $\theta'_{max} = -\xi/2 + \psi_o$ ) for which diffraction efficiency is maximized is shown in Fig. 8(c). When the grating is parallel to the  $[110]$  axis,  $\theta'_{max}$  undergoes a  $\pi/2$  phase jump and  $\eta_{ac} = 0$  for both cases.

In order to examine the validity of the calculations for the polarization of the diffracted beam, a grating is recorded at a fixed angle  $\gamma = +15^\circ$  from the  $[110]$  axis with  $E_o = 8$  kV/cm. During readout bias fields of (a)  $E_o = -8$  kV/cm and (b)  $E_o = 0$  kV/cm are applied along  $[110]$  as well. The  $\gamma = +15^\circ$  angle is chosen in order to examine the most general case where  $\mathbf{G}$ , and consequently  $\mathbf{E}_{sc}$ , are not parallel to  $\mathbf{E}_o$  [see Fig. 3(a)], while, on the other hand, to maintain high diffraction efficiency. The experimental and theoretical results for azimuth  $\psi_{az}$  and squared ellipticity  $\varepsilon_o^2$  of the diffracted beam versus input polarization direction are presented in Fig. 9.

The more recent  $(111)$  cut exhibits generally an  $120^\circ$  periodicity because  $[111]$  axis possesses threefold rotation axis. However, in our experiments this property is defeated by the influence of the externally applied electric field for recording. All the same, the external field which is applied during recording is  $E_o = +8$  kV/cm, and during readout it is  $E_o = -8$  kV/cm and  $E_o = 0$  kV/cm. The results for the DE and  $\theta'_{max}$  are shown in Fig. 10. It is noticed that  $\eta_{dc}$  is symmetric around  $\gamma = 0$  and is increased almost 20%, while the “left” ( $\gamma < 0$ ) lobe of  $\eta_{ac}$  is slightly decreased for no-applied field and is dramatically decreased when  $E_o = -8$  kV/cm is applied. When the grating is parallel to the  $[\bar{1}10]$ ,  $[\bar{1}01]$ , and  $[0\bar{1}1]$  directions,  $\pi/2$  phase jumps are occurring in  $\theta'_{max}$  and  $\eta_{ac}$  is zero again. The results for the azimuth and the squared ellipticity versus  $\theta'$  for a grating recorded at  $\gamma = 15^\circ$  to  $[\bar{1}10]$  are shown in Fig. 11. There is a good qualitative and quantitative agreement between theoretical and experimental results for both cuts and small mismatch is attributed to low diffraction efficiency values, which result in small signal to noise ratio and to a probable nonuniformity of the electric field. For both crystal cuts that were examined we can conclude that the application of external electric field increases the dc part of the de and decreases the ac part asymmetrically.

In order to establish the previous conclusion an experiment measuring the DE versus the applied field during readout is arranged for both crystal cuts. The grating vector is recorded along the direction  $\gamma = \gamma_{opt}$  for which DE is maxi-

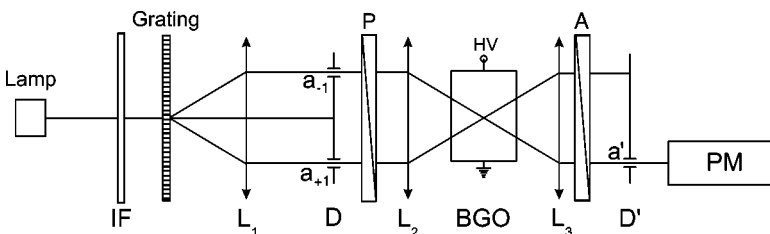


FIG. 6. Schematic diagram of the experimental setup. IF (interference filter);  $L_1$ ,  $L_2$ ,  $L_3$  (lenses);  $D$  and  $D'$  (Fourier planes),  $a_{+1}$ ,  $a_{-1}$ , and  $a'$  (apertures),  $P$  (polarizer—not used during the recording process);  $A$  (analyzer), and PM (photomultiplier)

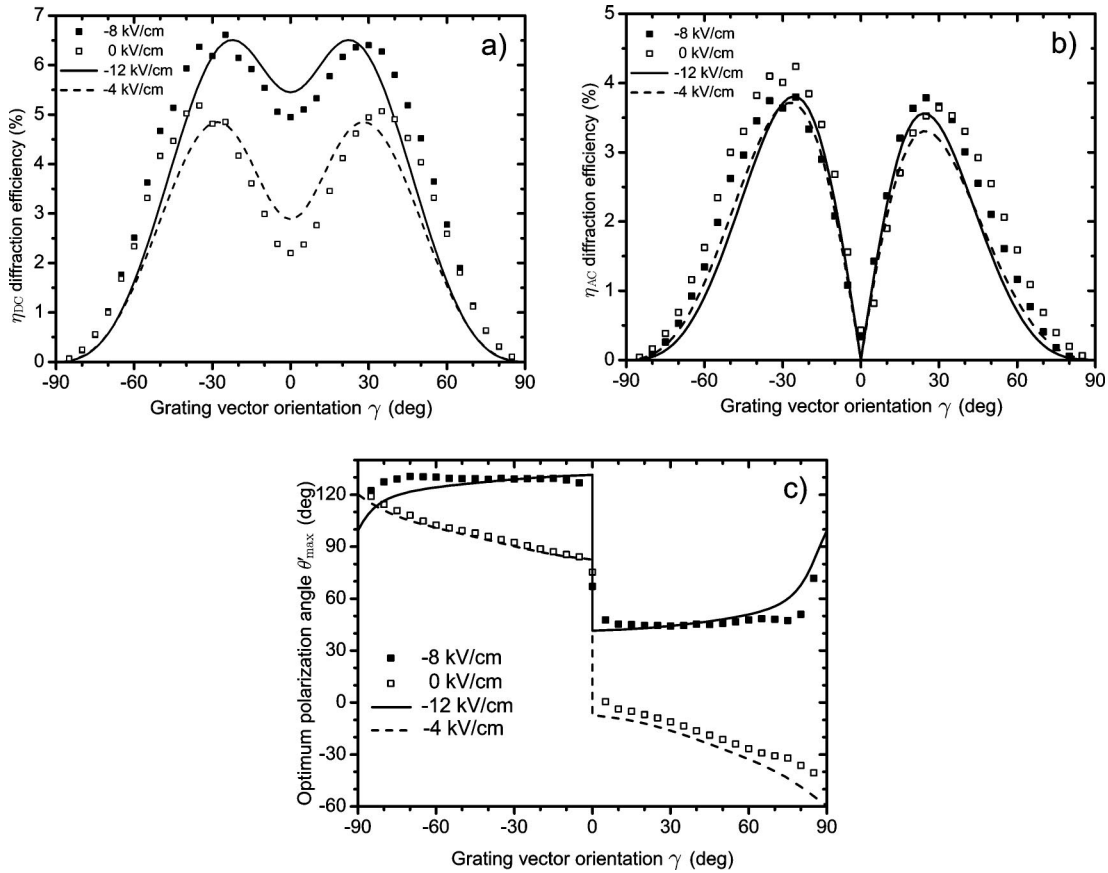


FIG. 8. Diffraction efficiency vs grating vector orientation for a 5.5 mm thick  $(1\bar{1}0)$ -cut positive BGO for  $E_o = -8$  kV/cm and  $0$  kV/cm external applied field. (a)  $\eta_{dc}$ , (b)  $\eta_{ac}$ , and (c) optimum input polarization angle  $\theta'_{max}$ . The theoretical curves are plotted for  $\alpha = 0.6$  and for  $E_o = -12$  kV/cm and  $-4$  kV/cm, respectively.

mized. DE is symmetric [ $\eta_{ac}(\gamma) = \eta_{ac}(-\gamma)$  and  $\eta_{dc}(\gamma) = \eta_{dc}(-\gamma)$ ] when no bias is applied and the optimum value is  $\gamma = \pm 43^\circ$  for the 5.5mm  $(1\bar{1}0)$ -cut and  $\gamma = \pm 30^\circ$  for the  $(111)$ -cut BGO crystal [31]. The  $\pm$  values are corresponding

to the maxima on either side  $\gamma > 0$  and  $\gamma < 0$  of  $\eta_{ac}$ . In Fig. 12  $\eta_{dc}$  and  $\eta_{ac}$  versus  $E_o$  are presented for two grating vector orientations. The two different ac parts belong to the two different lobes of the  $\eta_{ac}$  shown in Figs. 8(a) and 8(b). The

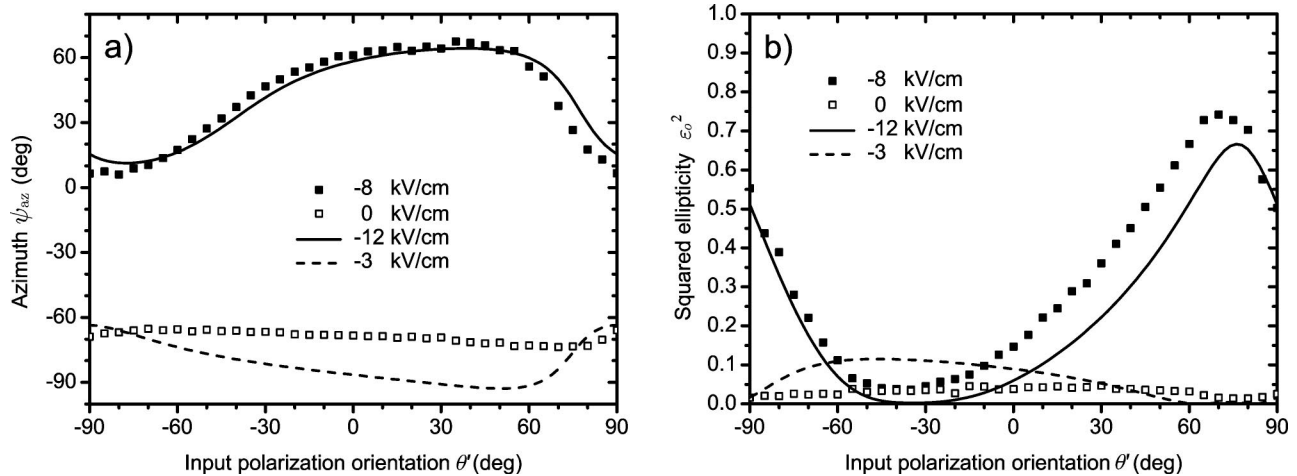


FIG. 9. Polarization state of the beam which is diffracted from a grating recorded at  $\gamma = +15^\circ$  from the  $[110]$  for a 5.5 mm thick  $(1\bar{1}0)$ -cut positive BGO for  $E_o = -8$  kV/cm and  $0$  kV/cm external applied field. (a) Azimuth angle  $\psi_{az}$  and (b) squared ellipticity  $\epsilon_o^2$ . The theoretical curves are plotted and for  $E_o = -12$  kV/cm and  $-3$  kV/cm, respectively.

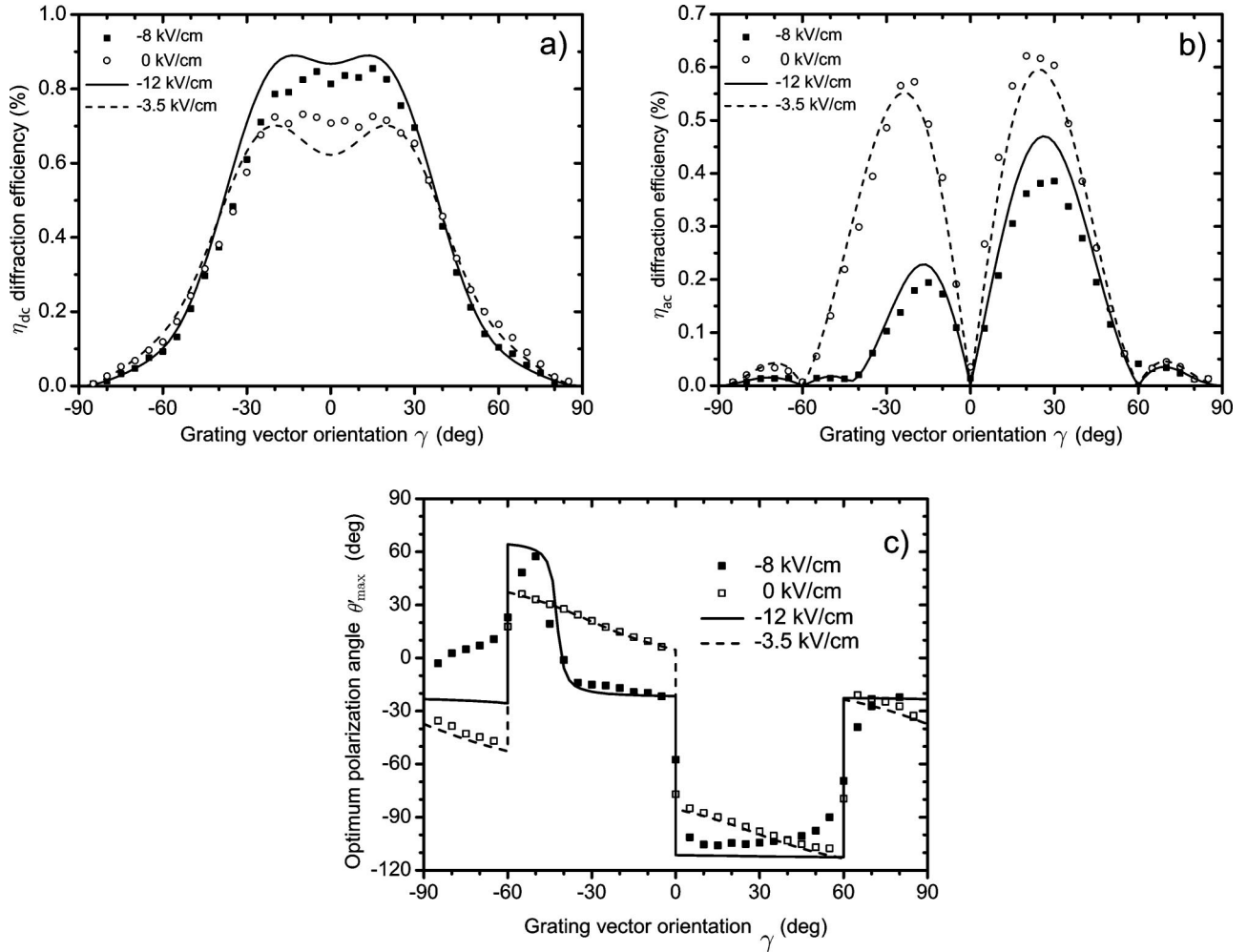


FIG. 10. Diffraction efficiency vs grating vector orientation for a 5 mm thick (111)-cut negative BGO for  $E_o = -8$  kV/cm and 0 kV/cm external applied field. (a)  $\eta_{dc}$ , (b)  $\eta_{ac}$ , and (c) optimum input polarization angle  $\theta'_{max}$ . The theoretical curves are plotted for  $\alpha = 0.33$  and for  $E_o = -12$  kV/cm and  $-3.5$  kV/cm, respectively.

dc part is gradually increasing but the two lobes are decreasing asymmetrically up to 8 kV/cm and then increasing, but it is always  $\eta_{ac}(-43^\circ) > \eta_{ac}(+43^\circ)$ . The experimental data are shifted along the horizontal axis by +3 kV/cm in order to compensate for the screening field. The same phenomenon is observed at the (111)-cut BGO (see Fig. 13). In this case the experimental data are shifted by +4 kV/cm. The  $\eta_{dc}$  is increasing but the two  $\eta_{ac}$  lobes decrease and increase asymmetrically. But this time, contrary to the (1 $\bar{1}$ 0) cut, it is  $\eta_{ac}(-30^\circ) < \eta_{ac}(+30^\circ)$ . This difference between the two cuts is attributed to the opposite sense of the rotatory power  $\varrho$  of the two BGO samples. If we change the sign of  $\varrho$  then the inequalities are reversed. The experimental results for both cases are in agreement with the theoretical and with the results obtained in the previous experiments of DE versus  $\gamma$ .

## VI. DISCUSSION ON THE ARBITRARY CUT

### A. Diffraction properties under inversion of the electric field

In order to read into the diffraction properties of the grating we should examine the influence of the inversion of electric field on the DE and the polarization of the diffracted

beam. This is important especially in experiments where alternating electric fields are applied. The formulas describing DE and the auxiliary parameters  $p$ ,  $q$ , and  $s$  in Eqs. (A3) depend on the space charge field  $\mathbf{E}_{sc}$  and on the externally applied field  $\mathbf{E}_o$ . Analysis shows that all the above formulas are even functions of the space charge field  $E_{sc}$ . Consequently, there is no change in the diffracted beam for any crystal cut and configuration when  $E_{sc}$  switches polarity. That is only to be expected since changing the sign of  $E_{sc}$  is equivalent to an 180° grating displacement. In DE experiments any grating displacement is of no importance because only one beam is used for readout, in contrast to TWM where such a displacement with respect to the interference pattern of the two beams is significant.

The situation is a bit different when the polarity of the externally applied electric field is changed. When the input is linearly polarized ( $\varepsilon = 0$ ) DE is even function  $\eta(-E_o) = \eta(E_o)$ , but  $p$ ,  $q$ , and  $s$  are odd functions. Consequently, for any crystal cut and configuration, DE  $\eta$ , azimuth  $\psi_{az}$ , and ellipticity  $\varepsilon_o$  remain the same, and only the sense of rotation of the polarization state changes under switching the polarity of  $E_o$ . When the input is elliptically polarized ( $\varepsilon \neq 0$ ) the

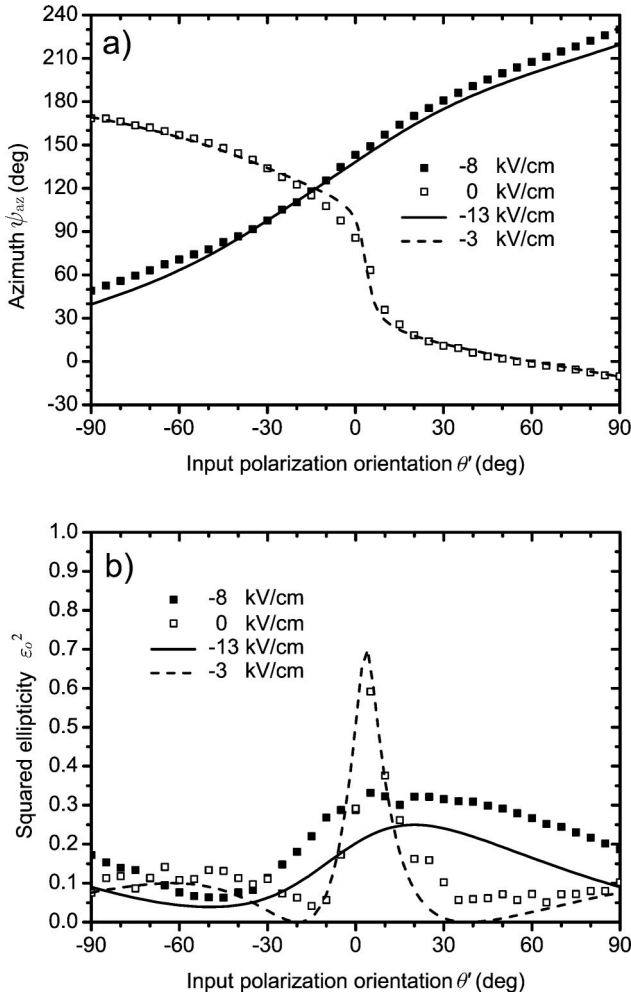


FIG. 11. Polarization state of the beam which is diffracted from a grating recorded at  $\gamma = +15^\circ$  from the  $[\bar{1}10]$  for a 5 mm thick (111)-cut negative BGO for  $E_o = -8$  kV/cm and 0 kV/cm external applied field. (a) Azimuth angle  $\psi_{az}$  and (b) squared ellipticity  $\epsilon_o^2$ . The theoretical curves are plotted and for  $E_o = -13$  kV/cm and  $-3$  kV/cm, respectively.

situation is somewhat more complicated. Each of the formulas for  $\eta$ ,  $p$ ,  $q$ , and  $s$  is decomposed into three parts; the first is constant and the second and third depend on  $\cos(2\theta)$  and  $\sin(2\theta)$ . When  $\epsilon \neq 0$ , an extra term appears on the constant term of each of the formulas above, which depends on the polarity of the external field and is proportional to  $\epsilon$ . Consequently  $\eta_{dc}$  has an extra term which is added/subtracted when the polarity of the applied field is positive/negative. On the other hand  $\psi_{az}$ ,  $\epsilon_o$ , and  $s$  get complicated. The above results are in agreement with those reported in Refs. [15,38].

**B. Diffraction efficiency independent of the orientation of the polarization at the input**

There are several cases in the literature where the output from a grating recorded in a sillenite crystal does not depend on the orientation  $\theta$  of the polarized light at the input [27,29,31,34,36,37,47,63,64]. This phenomenon is accompanied by the exhibition of  $\pi/2$  phase jumps on the  $\theta'_{max}$  plots

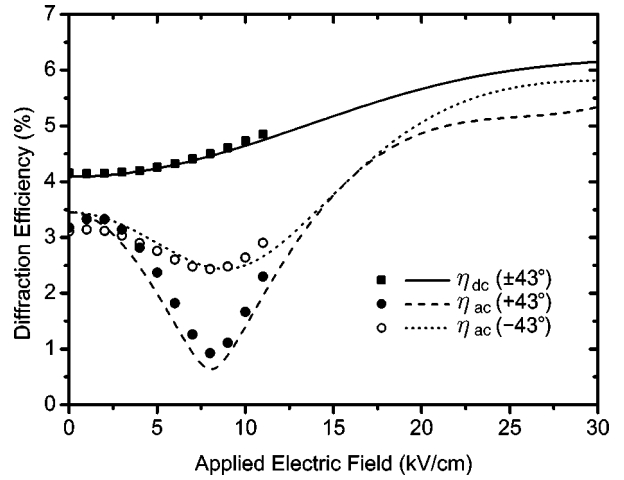


FIG. 12. DE vs electric field applied along  $[110]$  for a 5.5 mm  $(1\bar{1}0)$ -cut positive BGO crystal. The grating is recorded with  $E_o^e = +8$  kV/cm. (1)  $\eta_{dc}$  when  $\gamma = \pm 43^\circ$ , (2)  $\eta_{ac}$  when  $\gamma = +43^\circ$ , and (3)  $\eta_{dc}$  when  $\gamma = -43^\circ$ . Experimental data are shifted by  $+3$  kV/cm.

in Figs. 8(c) and 10(c) and it happens on two occasions: when  $\varrho L = 0, \pi, 2\pi, \dots$ , and when the grating vector is parallel to particular directions regardless of crystal thickness  $L$ . The former can be observed both in gain and diffraction efficiency investigations and is due to the fact that the light passes through all possible polarization states while propagating along crystal depth [27]. The latter is found only in DE experiments when the grating vector  $\mathbf{G}_{min}$  satisfies the condition  $|\Delta n_{x_{sc}}^o| = |\Delta n_{z_{sc}}^o|$  which is derived from Eqs. (A2b) and (A2c). This means that diffraction efficiency is the same along either of the principal diffracting axes of the modulated indicatrix (i.e.,  $Ox_{sc}$  and  $Oz_{sc}$ , see Fig. 5). Therefore, the elliptically polarized light that is incident on the elementary grating splits into the two diffracting axes  $Ox_{sc}$  and  $Oz_{sc}$

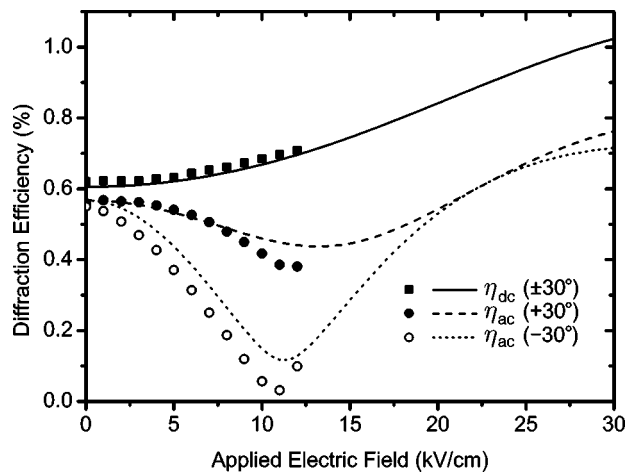


FIG. 13. DE vs electric field applied along  $[\bar{1}10]$  for a 5 mm (111)-cut negative BGO crystal. The grating is recorded with  $E_o^e = +8$  kV/cm. (1)  $\eta_{dc}$  when  $\gamma = \pm 30^\circ$ , (2)  $\eta_{ac}$  when  $\gamma = +30^\circ$ , and (3)  $\eta_{dc}$  when  $\gamma = -30^\circ$ . Experimental data are shifted by  $+4$  kV/cm.

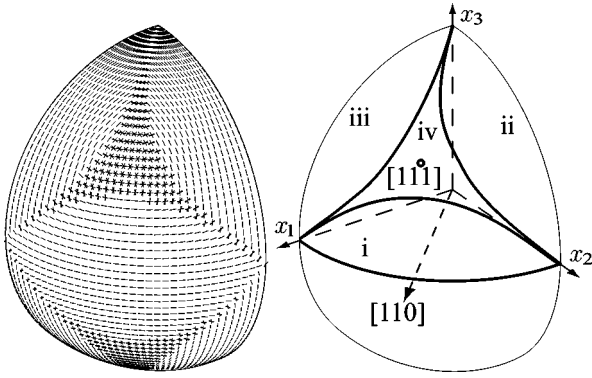


FIG. 14. Spherical grating vector orientation plot when DE is independent from  $\theta$ . The diagram is restricted to the first quarter for simplicity. In regions (i), (ii), and (iii) there are unique solutions which are roughly perpendicular to  $[001]$ ,  $[100]$ , and  $[010]$  axes, respectively. There are three solutions over region (iv).

and the two components are equally diffracted. The diffraction process does not introduce an extra amplitude or phase difference between two diffracted components of the beam, and consequently they combine and the diffracted amplitude is independent from initial light polarization [ $\eta_{ac}(\mathbf{G}_{min}) = 0$ ] [31].

$\Delta n_{x_{sc}}^o$  and  $\Delta n_{z_{sc}}^o$  are neither functions of the externally applied electric field  $\mathbf{E}_o$ , nor of the crystal thickness  $L$ , and the specific  $\mathbf{G}_{min}$  vectors are characteristic of each crystal cut. In Fig. 14 those  $\mathbf{G}_{min}$  vectors are depicted in a spherical vector plot for arbitrary cut for a  $\text{Bi}_{12}\text{GeO}_{20}$  crystal. For each cut (i.e., for each light direction of propagation), a small line representing the vector is drawn onto the surface of a sphere which is parallel to  $\mathbf{G}_{min}$  and perpendicular to the radial direction of propagation. Each small line corresponds to two opposite equivalent orientations since an  $180^\circ$  rotation produces the same grating. The diagram is restricted to the first quarter; the other quarters can be reproduced by applying the symmetry elements of the class. The top part of the quarter shown in Fig. 14 which is restricted by the three principal axes can be divided in four regions. In the central region there are three vector orientations for which  $\eta_{ac} = 0$ , while in the three peripheral regions only unique solutions exist. It can be observed that the vector orientation on each peripheral region is roughly perpendicular to a principal crystallographic axis and that the central region is a mix of the adjacent peripheral ones altogether. On the boundaries between the regions, two out of the three solutions coincide and the number of vectors degenerates down to two. Finally the diagram exhibits the elements of symmetry (twofold and threefold axes) that are typical of the sillenite family.

It is interesting to study the diffraction efficiency when the  $\eta_{ac}(\mathbf{G}_{min}) = 0$  condition holds. In Fig. 15 the  $\eta(\mathbf{G}_{min})$  for a 5 mm BGO crystal of arbitrary cut is shown for linearly polarized input light ( $\varepsilon = 0$ ). Among the triplets of  $\mathbf{G}_{min}$  in the central region of Fig. 14 the ones that produce the highest DE were used for the calculation. The two cases presented are for 0 kV and 8 kV applied electric field along grating vector orientation. The DE surface consists of 12 lobes and exhibits the twofold and threefold symmetry rotations.

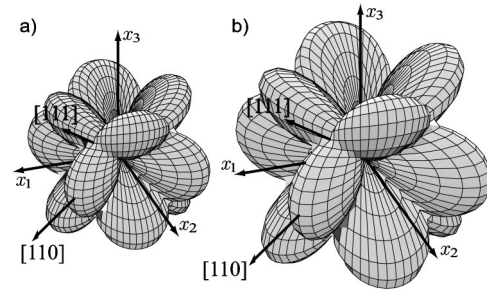


FIG. 15. DE for arbitrary direction of light propagation when  $\mathbf{G} = \mathbf{G}_{min}$  and output is independent of  $\theta$  for a 5 mm thick BGO crystal. (a)  $E_o = 0$  and (b)  $E_o = 8$  kV/cm and  $\mathbf{E}_o \parallel \mathbf{G}_{min}$ .

Maxima of DE are located along  $\langle 110 \rangle$  directions, and a kind of saddle points occur along the  $\langle 111 \rangle$  directions with DE being 66% compared to the maximum at  $\langle 110 \rangle$ . The application of external electric field along  $\mathbf{G}_{min}$  results in a DE surface with essentially the same shape, but the lobes are a bit more pronounced. The maxima at  $\langle 110 \rangle$  and the saddle point at  $\langle 111 \rangle$  are increased about 40% and 28%, respectively.

### C. Diffraction efficiency at optimum grating vector orientation $\mathbf{G}_{max}$

In this section we examine the diffraction efficiency at optimum grating orientation  $\mathbf{G}_{max}$  with and without applied electric field. The spherical vector orientation plot for maximum DE for arbitrary cut in a 5 mm BGO crystal is shown in Fig. 16. The top part of the quarter shown can be divided into three areas and a threefold rotation axis exists along the  $[111]$  direction. In each area only unique solutions exist for which DE is optimized and they are roughly perpendicular to the  $\langle 110 \rangle$  directions. Double solutions appear along the boundary lines of the areas, triple solutions on the cross points along the  $\langle 111 \rangle$  directions.

In Fig. 17 the surfaces of the amplitude  $\eta_{ac}(\mathbf{G}_{max})$  and the constant part  $\eta_{dc}(\mathbf{G}_{max})$  for arbitrary cut and when no electric field is applied externally are depicted. The surfaces exhibit the twofold and threefold rotation axes as expected and

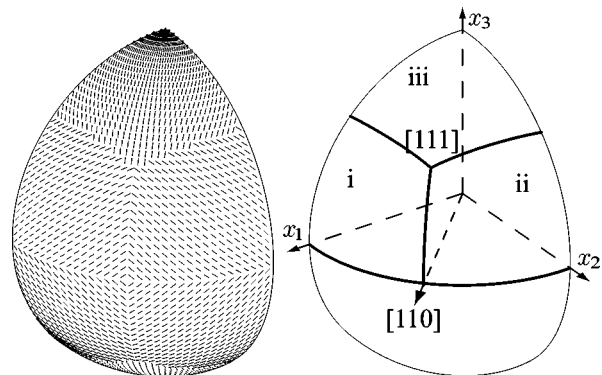


FIG. 16. Spherical grating vector orientation diagram for maximum DE independent from input polarization for a 5 mm BGO crystal. In regions (i), (ii), and (iii) the solutions are roughly perpendicular to  $[01\bar{1}]$ ,  $[\bar{1}01]$ , and  $[1\bar{1}0]$ , respectively.

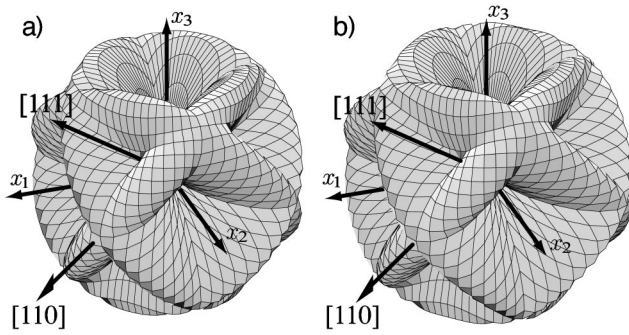


FIG. 17. DE for arbitrary direction of light propagation for a 5 mm thick BGO crystal when  $\mathbf{G}=\mathbf{G}_{\max}$  and  $E_o=0$ . (a)  $\eta_{ac}(\mathbf{G}_{\max})$  and (b)  $\eta_{dc}(\mathbf{G}_{\max})$ .

they have essentially the same shape. The absolute maxima appear along the  $\langle 110 \rangle$  directions local minima exist along the  $\langle 111 \rangle$  directions, being 41% and 43% of the maxima for  $\eta_{ac}(\mathbf{G}_{\max})$  and  $\eta_{dc}(\mathbf{G}_{\max})$ , respectively. The  $\eta_{dc}(\mathbf{G}_{\max})/\eta_{ac}(\mathbf{G}_{\max})$  ratio ranges between 1 and 1.19 and its values for the  $\langle 110 \rangle$  and  $\langle 111 \rangle$  directions are 1.07 and 1.10, respectively. The above surfaces are similar to the one calculated by Kamenov *et al.* for TWM gain when  $E_o=0$  and  $qL=\pi$  [47].

In Fig. 18 the DE efficiency surfaces are calculated as above but for an 8 kV/cm electric field applied along the optimum grating direction  $\mathbf{G}_{\max}$ . The shape of the surfaces remain the same as before but there is an obvious shrinking of the AC term and an expansion of the dc surface. The  $\eta_{dc}(\mathbf{G}_{\max})/\eta_{ac}(\mathbf{G}_{\max})$  ratio ranges between 1 and 2.1 and it is 1.87 and 2.1 for the  $\langle 110 \rangle$  and  $\langle 111 \rangle$  directions, respectively. The maximum DE  $\eta(\mathbf{G}_{\max})=\eta_{dc}(\mathbf{G}_{\max})+\eta_{ac}(\mathbf{G}_{\max})$  when  $E_o=8$  kV/cm is applied turns out to be a bit lower compared to the case when no electric field is applied for every crystal cut. The worst case is the  $\{111\}$  cuts where DE is 86% of the original.

## VII. CONCLUSIONS

In this paper we have presented a comprehensive analytical model on the diffraction from gratings recorded in sille-

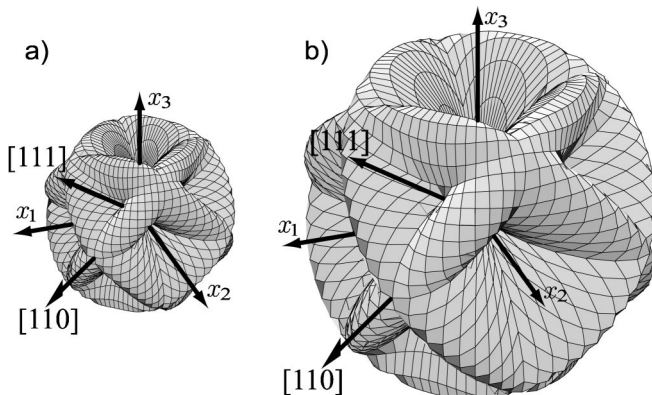


FIG. 18. DE for arbitrary direction of light propagation for a 5 mm thick BGO crystal when  $\mathbf{G}=\mathbf{G}_{\max}$  and  $E_o=8$  kV/cm and  $\mathbf{E}_o\parallel\mathbf{G}_{\max}$ . (a)  $\eta_{ac}(\mathbf{G}_{\max})$  and (b)  $\eta_{dc}(\mathbf{G}_{\max})$ .

nite crystals. The theory is based on the analysis of the volume grating into elementary slices inside the crystal which diffract the light. The calculations are performed for arbitrary crystal cut taking into account optical activity and the induced birefringence coming from the externally applied electric field, as well as the influence of the piezoelectric effect. We assume an undepleted pump beam that propagates at small angle to the normal of the input face (paraxial beam approximation). Emphasis is given so that the resulting formulas for diffraction efficiency and the polarization state of the diffracted beam are expressed on the original parameters of the problem (i.e., input polarization ellipticity  $\varepsilon$  and azimuth  $\theta$ , eigenpolarization ellipticity  $k$ , and refractive index change  $\Delta n_{x,z_{sc}}$ ). The experimental results are in good agreement with the predictions from theory. It should be noted that during the recording of a grating an inverse electric field builds up which decreases the effective value of the externally applied field. Here we summarize some of the results deduced from the analysis of the theory:

(1) The piezoelectric effect influences both the electro-optic coefficient and the effective static dielectric permittivity. In the latter, the piezoelectric effect increases the static dielectric permittivity, which results in the reduction of the original value of the space charge field. The reduction depends on the orientation of the grating and it can be up to 8%.

(2) In general, DE consists of a mean value ( $\eta_{dc}$ ) and a part which depends on the orientation of polarization of the readout beam ( $\eta_{ac}$ ). The external application of the electric field bias up to 8 kV/cm along the optimum grating vector direction increases  $\eta_{dc}$ , and decreases  $\eta_{ac}$ .

(3) For each crystal cut there are one to three grating vector directions for which the diffraction efficiency is independent of the linear polarization of the input.

(4) When the space charge field switches polarity, the diffraction efficiency of the grating and the polarization of the diffracted beam remain the same. When the polarity of the external field is switched and the read out beam is linearly polarized, the DE, the azimuth, and ellipticity of the diffracted beam remain the same, and only its sense of rotation switches.

Finally, the analytical solution of the diffraction properties of thick phase gratings recorded in sillenite crystals makes it possible to investigate in depth the influence of various parameters on the phenomenon and to optimize their performance in several applications.

## ACKNOWLEDGMENT

One of the authors (N.C.D.) is supported by the Greek State Scholarship Foundation.

## APPENDIX

The light electric field  $\mathbf{U}_o(L)$  of the diffracted beam is given in Eq. (29), where  $A$ ,  $B$ ,  $C$ , and  $D$  are

$$\begin{aligned}
 A = & \frac{\pi P_o}{2\phi\lambda(k^2+1)^2\sqrt{\varepsilon^2+1}} \left[ (\Delta n_{x_{sc}} - \Delta n_{z_{sc}}) \cos(2\Delta\psi) (\sin\theta [\phi L(k^2-1)(k-k^2\varepsilon) + \phi L(k^2-1)(k+\varepsilon) \cos\phi L \right. \\
 & - 2k(k^2+2k\varepsilon-1) \sin\phi L] + \cos\theta \{2k[2k+(k^2-1)\varepsilon] (\cos\phi L-1) + \phi L(k^2-1)(k\varepsilon+1) \sin\phi L\} \\
 & + 2(k^2+1)^2 (\Delta n_{x_{sc}} - \Delta n_{z_{sc}}) \sin 2\Delta\psi \sin \frac{\phi L}{2} \left( \varepsilon \cos\theta \cos \frac{\phi L}{2} - \sin\theta \sin \frac{\phi L}{2} \right) + \phi L(k^2+1) (\Delta n_{x_{sc}} + \Delta n_{z_{sc}}) \\
 & \left. \times \{ [k-k^2\varepsilon - (k+\varepsilon) \cos\phi L] \sin\theta - (k\varepsilon+1) \cos\theta \sin\phi L \} \right], \quad (A1a)
 \end{aligned}$$

$$\begin{aligned}
 B = & \frac{-\pi P_o}{2\phi\lambda(k^2+1)^2\sqrt{\varepsilon^2+1}} \left[ (\Delta n_{x_{sc}} - \Delta n_{z_{sc}}) \cos(2\Delta\psi) (\cos\theta \{ \phi L(1-k^2)[k\varepsilon-k^2+(k\varepsilon+1) \cos\phi L] + 2k(k^2\varepsilon \right. \\
 & + 2k-\varepsilon) \sin\phi L \} + \sin\theta [2k(k^2+2k\varepsilon-1) (\cos\phi L-1) + (k^2-1)L(k+\varepsilon) \phi \sin\phi L]) + (k^2+1)^2 \\
 & \times (\Delta n_{x_{sc}} - \Delta n_{z_{sc}}) \sin 2\Delta\psi \left( 2\varepsilon \cos\theta \sin^2 \frac{\phi L}{2} + \sin\theta \sin\phi L \right) + \phi L(k^2+1) (\Delta n_{x_{sc}} + \Delta n_{z_{sc}}) \\
 & \left. \times \{ \cos\theta [k^2-k\varepsilon + (k\varepsilon+1) \cos\phi L] - (k+\varepsilon) \sin\theta \sin\phi L \} \right], \quad (A1b)
 \end{aligned}$$

$$\begin{aligned}
 C = & \frac{\pi P_o}{2\phi\lambda(k^2+1)^2\sqrt{\varepsilon^2+1}} \left[ (\Delta n_{x_{sc}} - \Delta n_{z_{sc}}) \cos(2\Delta\psi) (\cos\theta \{ \phi L(1-k^2)[k-\varepsilon + (k+k^2\varepsilon) \cos\phi L] + 2k(k^2-2k\varepsilon-1) \sin\phi L \} \right. \\
 & + \sin\theta [2k(k^2\varepsilon-2k-\varepsilon) (\cos\phi L-1) + \phi Lk(k^2-1)(k+\varepsilon) \sin\phi L]) - (k^2+1)^2 (\Delta n_{x_{sc}} - \Delta n_{z_{sc}}) \sin 2\Delta\psi \\
 & \times [\cos\theta (1-\cos\phi L) + \varepsilon \sin\theta \sin\phi L] + \phi L(k^2+1) (\Delta n_{x_{sc}} + \Delta n_{z_{sc}}) \{ \cos\theta [\varepsilon-k + (k+k^2\varepsilon) \cos\phi L] \\
 & \left. - (k^2+k\varepsilon) \sin\theta \sin\phi L \} \right], \quad (A1c)
 \end{aligned}$$

$$\begin{aligned}
 D = & \frac{-\pi P_o}{2\phi\lambda(k^2+1)^2\sqrt{\varepsilon^2+1}} \left[ (\Delta n_{x_{sc}} - \Delta n_{z_{sc}}) \cos(2\Delta\psi) (\sin\theta \{ \phi L(k^2-1)[1-k\varepsilon - k(k+\varepsilon) \cos\phi L] + 2k(k^2\varepsilon-2k-\varepsilon) \sin\phi L \} \right. \\
 & + \cos\theta [2k(k^2-2k\varepsilon-1)(1-\cos\phi L) - \phi Lk(k^2-1)(k\varepsilon+1) \sin\phi L]) + 2(k^2+1)^2 \\
 & \times (\Delta n_{x_{sc}} - \Delta n_{z_{sc}}) \sin 2\Delta\psi \sin \frac{\phi L}{2} \left( \cos\theta \cos \frac{\phi L}{2} - \varepsilon \sin\theta \sin \frac{\phi L}{2} \right) + \phi L(k^2+1) (\Delta n_{x_{sc}} + \Delta n_{z_{sc}}) \\
 & \left. \times \{ [1-k\varepsilon + k(k+\varepsilon) \cos\phi L] \sin\theta + (k+k^2\varepsilon) \cos\theta \sin\phi L \} \right]. \quad (A1d)
 \end{aligned}$$

The dc and ac parts of the diffraction efficiency  $\eta$  in Eq. (31) are

$$\begin{aligned}
 \eta_{dc} = & \frac{\pi^2}{8\phi^2\lambda^2(1+k^2)^2(\varepsilon^2+1)} \left\{ (\varepsilon^2+1) \{ 2(k^4+6k^2+1) (\Delta n_{x_{sc}} - \Delta n_{z_{sc}})^2 + \phi^2 L^2 [(3k^4+2k^2+3) (\Delta n_{x_{sc}}^2 + \Delta n_{z_{sc}}^2) \right. \\
 & + 2(k^4+6k^2+1) \Delta n_{x_{sc}} \Delta n_{z_{sc}}] \} + (\Delta n_{x_{sc}} - \Delta n_{z_{sc}})^2 (\varepsilon^2+1) [(k^2-1)^2 \cos 4\Delta\psi (\phi^2 L^2 + 2\cos\phi L - 2) \\
 & \left. - 2(k^4+6k^2+1) \cos\phi L] + 16\varepsilon \phi L(k^2-1) (\Delta n_{x_{sc}}^2 - \Delta n_{z_{sc}}^2) \left[ (k^2+1) \sin 2\Delta\psi \sin^2 \frac{\phi L}{2} + k \cos 2\Delta\psi (\sin\phi L - \phi L) \right] \right\}, \quad (A2a)
 \end{aligned}$$

$$\eta_{ac1} = \frac{\pi^2 L (\Delta n_{x_{sc}}^2 - \Delta n_{z_{sc}}^2) (1-\varepsilon^2)}{2\phi\lambda^2(1+k^2)^2(\varepsilon^2+1)} \left\{ 4(k^3+k) \sin 2\Delta\psi \sin^2 \frac{\phi L}{2} + \cos 2\Delta\psi [\phi L(k^2-1)^2 + 4k^2 \sin\phi L] \right\}, \quad (A2b)$$

$$\eta_{ac_2} = \frac{\pi^2 L (\Delta n_{x_{sc}}^2 - \Delta n_{z_{sc}}^2) (\varepsilon^2 - 1)}{2 \phi \lambda^2 (1 + k^2) (\varepsilon^2 + 1)} \left[ 4k \cos 2\Delta\psi \sin^2 \frac{\phi L}{2} - (k^2 + 1) \sin 2\Delta\psi \sin \phi L \right]. \quad (A2c)$$

Similarly to Eq. (31), the  $p$ ,  $q$ , and  $s$  parameters that describe the polarization of the diffracted beam consist of constant and  $\theta$  modulated parts:

$$\begin{aligned} p &= p_b + p_c \cos 2\theta + p_s \sin 2\theta, \\ q &= q_b + q_c \cos 2\theta + q_s \sin 2\theta, \\ s &= s_b + s_c \cos 2\theta + s_s \sin 2\theta, \end{aligned} \quad (A3)$$

where  $p_b$ ,  $p_c$ ,  $p_s$ ,  $q_b$ ,  $q_c$ ,  $q_s$ ,  $s_b$ ,  $s_c$ , and  $s_s$  are

$$\begin{aligned} p_b &= \frac{\pi^2 P_o^2 \sin(\phi L/2)}{4(k^2 + 1)^3 (\varepsilon^2 + 1) \lambda^2 \phi^2} \left( 2\phi L \cos \frac{\phi L}{2} \{ \varepsilon \phi L (k^2 - 1) [(k^4 + 6k^2 + 1)(\Delta n_{x_{sc}}^2 + \Delta n_{z_{sc}}^2) + (6k^4 + 4k^2 + 6)\Delta n_{x_{sc}} \Delta n_{z_{sc}}] \right. \\ &\quad + (\Delta n_{x_{sc}} - \Delta n_{z_{sc}}) [-\varepsilon \phi L (k^2 - 1)^3 (\Delta n_{x_{sc}} - \Delta n_{z_{sc}}) \cos 4\Delta\psi + 2(k^2 + 1)^3 (\Delta n_{x_{sc}} + \Delta n_{z_{sc}}) (\varepsilon^2 + 1) \sin 2\Delta\psi - 4\varepsilon k (k^4 - 1) \\ &\quad \times (\Delta n_{x_{sc}} - \Delta n_{z_{sc}}) \sin 4\Delta\psi] \} + 8k (\Delta n_{x_{sc}} - \Delta n_{z_{sc}}) \cos 2\Delta\psi \sin \frac{\phi L}{2} \{ \phi L (k^2 + 1)^2 (\Delta n_{x_{sc}} + \Delta n_{z_{sc}}) (\varepsilon^2 + 1) + 4\varepsilon (k^2 - 1) \\ &\quad \times (\Delta n_{x_{sc}} - \Delta n_{z_{sc}}) [(k^2 + 1) \sin 2\Delta\psi - k \phi L \cos 2\Delta\psi] \} \left. \right), \end{aligned}$$

$$\begin{aligned} p_c &= -\frac{\pi^2 P_o^2 (\varepsilon^2 - 1) \sin(\phi L/2)}{4(k^2 + 1)^3 (\varepsilon^2 + 1) \lambda^2 \phi^2} \left( 8k (\Delta n_{x_{sc}} - \Delta n_{z_{sc}})^2 \cos 2\Delta\psi [(k^2 - 1)^2 \phi L \cos 2\Delta\psi + 4k(k^2 + 1) \sin 2\Delta\psi] \sin \frac{\phi L}{2} \right. \\ &\quad + 2\phi L \cos \frac{\phi L}{2} \{ k \phi L [(k^4 + 6k^2 + 1)(\Delta n_{x_{sc}}^2 + \Delta n_{z_{sc}}^2) + (6k^4 + 4k^2 + 6)\Delta n_{x_{sc}} \Delta n_{z_{sc}}] + (k - 1)^2 (k + 1)^2 (\Delta n_{x_{sc}} - \Delta n_{z_{sc}})^2 \\ &\quad \times [(k^2 + 1) \sin 4\Delta\psi - k \phi L \cos 4\Delta\psi] \} \left. \right), \end{aligned}$$

$$\begin{aligned} p_s &= -\frac{\pi^2 P_o^2 (\varepsilon^2 - 1)}{(k^2 + 1)^2 (\varepsilon^2 + 1) \lambda^2 \phi^2} \left[ \cos^2 \Delta\psi \sin^2 \Delta\psi \{ \phi^2 L^2 [(k^4 + 1)(\Delta n_{x_{sc}}^2 + \Delta n_{z_{sc}}^2) + 4k^2 \Delta n_{x_{sc}} \Delta n_{z_{sc}}] \cos \phi L \right. \\ &\quad + (k^2 + 1)^2 (\Delta n_{x_{sc}} - \Delta n_{z_{sc}})^2 \sin^2 \phi L \} + \frac{1}{4} \phi^2 L^2 (k^2 \Delta n_{x_{sc}} + \Delta n_{z_{sc}}) (\Delta n_{x_{sc}} + k^2 \Delta n_{z_{sc}}) (3 + \cos 4\Delta\psi) \cos \phi L \\ &\quad \left. + (\Delta n_{x_{sc}} - \Delta n_{z_{sc}})^2 \sin^2 \frac{\phi L}{2} \left[ (k^2 + 1)^2 \sin^2 2\Delta\psi \sin^2 \frac{\phi L}{2} - 4k^2 \cos^2 2\Delta\psi \right] \right], \end{aligned}$$

$$\begin{aligned} q_b &= \frac{\pi^2 P_o^2}{2(k^2 + 1)^4 (\varepsilon^2 + 1) \lambda^2 \phi^2} \left[ -4\phi L k (k^2 + 1)^3 (\varepsilon^2 + 1) (\Delta n_{x_{sc}} - \Delta n_{z_{sc}}) (\Delta n_{x_{sc}} + \Delta n_{z_{sc}}) \sin 2\Delta\psi \sin^2 \frac{\phi L}{2} + 2\varepsilon \phi L (k^2 - 1) \right. \\ &\quad \times (k^2 + 1)^3 (\Delta n_{x_{sc}} - \Delta n_{z_{sc}})^2 \sin 4\Delta\psi \sin^2 \frac{\phi L}{2} + \phi L (k^2 + 1)^2 (\Delta n_{x_{sc}} - \Delta n_{z_{sc}}) (\Delta n_{x_{sc}} + \Delta n_{z_{sc}}) (\varepsilon^2 + 1) \cos 2\Delta\psi [\phi L (k^2 - 1)^2 \\ &\quad + 4k^2 \sin \phi L] - \varepsilon k (k^2 - 1) (\Delta n_{x_{sc}} - \Delta n_{z_{sc}})^2 \cos 4\Delta\psi \left[ 2\phi^2 L^2 (k^2 - 1)^2 \cos \frac{\phi L}{2} - 32k^2 \sin^2 \frac{\phi L}{2} - 2\phi L (k^4 - 6k^2 + 1) \sin \phi L \right] \\ &\quad + \varepsilon k ((k^2 - 1) \{ 16k^2 (\Delta n_{x_{sc}} - \Delta n_{z_{sc}})^2 - \phi^2 L^2 [(3k^4 + 2k^2 + 3)(\Delta n_{x_{sc}}^2 + \Delta n_{z_{sc}}^2) + 2(k^4 + 6k^2 + 1)\Delta n_{x_{sc}} \Delta n_{z_{sc}}] \} \\ &\quad + 2\phi L (k^6 - 7k^4 + 7k^2 - 1) (\Delta n_{x_{sc}} - \Delta n_{z_{sc}})^2 \sin \phi L + (k^2 - 1) \{ \phi^2 L^2 [(k^4 + 6k^2 + 1)(\Delta n_{x_{sc}}^2 + \Delta n_{z_{sc}}^2) \\ &\quad + (6k^4 + 4k^2 + 6)\Delta n_{x_{sc}} \Delta n_{z_{sc}}] - 16k^2 (\Delta n_{x_{sc}} - \Delta n_{z_{sc}})^2 \} \cos \phi L \left. \right], \end{aligned}$$

$$\begin{aligned}
q_c &= \frac{\pi^2 P_o^2 (\varepsilon^2 - 1)}{8(k^2 + 1)^4 (\varepsilon^2 + 1) \lambda^2 \phi^2} \left( (k^2 - 1)^2 \{ 2(1 + 10k^2 + k^4) (\Delta n_{x_{sc}} - \Delta n_{z_{sc}})^2 - \phi^2 L^2 [(3k^4 + 2k^2 + 3) (\Delta n_{x_{sc}}^2 + \Delta n_{z_{sc}}^2) \right. \\
&\quad + 2(k^4 + 6k^2 + 1) \Delta n_{x_{sc}} \Delta n_{z_{sc}}] \} - 2 \{ (k^2 - 1)^2 (k^4 + 10k^2 + 1) (\Delta n_{x_{sc}} - \Delta n_{z_{sc}})^2 + 2k^2 \phi^2 L^2 [(k^4 + 6k^2 + 1) (\Delta n_{x_{sc}}^2 + \Delta n_{z_{sc}}^2) \\
&\quad + 2(3k^4 + 2k^2 + 3) \Delta n_{x_{sc}} \Delta n_{z_{sc}}] \} \cos \phi L + (\Delta n_{x_{sc}} - \Delta n_{z_{sc}})^2 \cos 4\Delta\psi \{ -2(k^8 + 30k^4 + 1) - \phi^2 L^2 (k^2 - 1)^4 \\
&\quad + 2[k^8 + 30k^4 + 1 + 2\phi^2 L^2 (k^3 - k)^2] \cos \phi L - 16\phi L (k - k^3)^2 \sin \phi L \} - 16\phi L (k - k^3)^2 (\Delta n_{x_{sc}} - \Delta n_{z_{sc}})^2 \sin \phi L \Big), \\
q_s &= -\frac{\pi^2 P_o^2 (\varepsilon^2 - 1) \sin(\phi L/2)}{4(k^2 + 1)^3 (\varepsilon^2 + 1) \lambda^2 \phi^2} \left[ -2k \phi^2 L^2 [(k^4 + 6k^2 + 1) (\Delta n_{x_{sc}}^2 + \Delta n_{z_{sc}}^2) + 2(3k^4 + 2k^2 + 3) \Delta n_{x_{sc}} \Delta n_{z_{sc}}] \cos \frac{\phi L}{2} \right. \\
&\quad + 2(\Delta n_{x_{sc}} - \Delta n_{z_{sc}})^2 \left( \phi L (k^2 - 1)^2 \cos \frac{\phi L}{2} [k \phi L \cos 4\Delta\psi + (k^2 + 1) \sin 4\Delta\psi] - 4k \cos 2\Delta\psi [\phi L (k^2 - 1)^2 \cos 2\Delta\psi - 4k \right. \\
&\quad \left. \left. \times (k^2 + 1) \sin 2\Delta\psi] \sin \frac{L\phi}{2} \right) \right], \\
s_b &= \frac{\pi^2 P_o^2}{8(k^2 + 1)^4 (\varepsilon^2 + 1) \lambda^2 \phi^2} \left( \varepsilon \{ (k^2 - 1)^2 (\Delta n_{x_{sc}} - \Delta n_{z_{sc}})^2 \cos 4\Delta\psi \{ 2[k^4 + 1 + 2k^2(5 + \phi^2 L^2)] - [2(k^4 + 10k^2 + 1) + \phi^2 L^2 \right. \\
&\quad \left. \times (k^2 - 1)^2] \cos \phi L \} + \{ 2(k^8 + 30k^4 + 1) (\Delta n_{x_{sc}} - \Delta n_{z_{sc}})^2 + \phi^2 L^2 (k^2 - 1)^2 [(k^4 + 6k^2 + 1) (\Delta n_{x_{sc}}^2 + \Delta n_{z_{sc}}^2) \right. \\
&\quad + 2(3k^4 + 2k^2 + 3) \Delta n_{x_{sc}} \Delta n_{z_{sc}}] \} \cos \phi L - 2(k^8 + 30k^4 + 1) (\Delta n_{x_{sc}} - \Delta n_{z_{sc}})^2 + 4k^2 \phi^2 L^2 [(3k^4 + 2k^2 + 3) (\Delta n_{x_{sc}}^2 \Delta n_{z_{sc}}^2) \\
&\quad + 2(k^4 + 6k^2 + 1) \Delta n_{x_{sc}} \Delta n_{z_{sc}}] \} - 4\phi L (k^2 - 1) (k^2 + 1)^3 (\Delta n_{x_{sc}}^2 - \Delta n_{z_{sc}}^2) (\varepsilon^2 + 1) \sin 2\Delta\psi \sin^2 \frac{\phi L}{2} - 32\varepsilon \phi L (k^3 - k)^2 \\
&\quad \left. \times (\Delta n_{x_{sc}} - \Delta n_{z_{sc}})^2 \cos 2\Delta\psi^2 \sin \phi L + 4k \phi L (k^2 - 1) (k^2 + 1)^2 (\varepsilon^2 + 1) (\Delta n_{x_{sc}}^2 - \Delta n_{z_{sc}}^2) \cos 2\Delta\psi [-\phi L + \sin \phi L] \right), \\
s_c &= \frac{\pi^2 P_o^2 (k^2 - 1) (\varepsilon^2 - 1)}{8(k^2 + 1)^4 (\varepsilon^2 + 1) \lambda^2 \phi^2} \left[ -k \{ -16k^2 (\Delta n_{x_{sc}} - \Delta n_{z_{sc}})^2 + \phi^2 L^2 [(k^4 + 6k^2 + 1) (\Delta n_{x_{sc}}^2 + \Delta n_{z_{sc}}^2) \right. \\
&\quad + 2(3k^4 + 2k^2 + 3) \Delta n_{x_{sc}} \Delta n_{z_{sc}}] \} \cos \phi L + k \phi^2 L^2 [(3k^4 + 2k^2 + 3) (\Delta n_{x_{sc}}^2 + \Delta n_{z_{sc}}^2) + 2(k^4 + 6k^2 + 1) \Delta n_{x_{sc}} \Delta n_{z_{sc}}] \\
&\quad + 2\phi L (\Delta n_{x_{sc}} - \Delta n_{z_{sc}})^2 \left( (k^2 + 1)^3 \sin 4\Delta\psi \sin^2 \frac{\phi L}{2} - (k^5 - 6k^3 + k) \sin \phi L \right) + 2(\Delta n_{x_{sc}} - \Delta n_{z_{sc}})^2 \cos 4\Delta\psi \\
&\quad \left. \times \left( \phi^2 L^2 k (k^2 - 1)^2 \cos \frac{\phi L}{2} - 16k^3 \sin^2 \frac{\phi L}{2} - \phi L (k^5 - 6k^3 + k) \sin \phi L \right) - 16k^3 (\Delta n_{x_{sc}} - \Delta n_{z_{sc}})^2 \right], \\
s_s &= \frac{\pi^2 P_o^2 (\varepsilon^2 - 1) \sin(\phi L/2)}{8(k^2 + 1)^3 (\varepsilon^2 + 1) \lambda^2 \phi^2} \left( \phi L \cos \frac{\phi L}{2} \{ \phi L (k^2 - 1) [(k^4 + 6k^2 + 1) (\Delta n_{x_{sc}}^2 + \Delta n_{z_{sc}}^2) + 2(3k^4 + 2k^2 + 3) \Delta n_{x_{sc}} \Delta n_{z_{sc}}] \right. \\
&\quad + (\Delta n_{x_{sc}} - \Delta n_{z_{sc}})^2 [-\phi L (k^2 - 1)^3 \cos 4\Delta\psi + 4k(k^4 - 1) \sin 4\Delta\psi] \} - 16k(k^2 - 1) (\Delta n_{x_{sc}} - \Delta n_{z_{sc}})^2 \cos 2\Delta\psi \\
&\quad \left. \times [\phi L k \cos 2\Delta\psi + (k^2 + 1) \sin 2\Delta\psi] \sin \frac{\phi L}{2} \right).
\end{aligned}$$

[1] *Photorefractive Materials and Their Applications, I and II*, Topics in Applied Physics, Vol. 61, edited by P. Gunter and J. Huignard (Springer-Verlag, Berlin, 1988).

[2] L. Solymar, D.J. Webb, and A. Grunnet-Jepsen, *The Physics*

*and Applications of Photorefractive Materials* (Clarendon Press, Oxford, 1996).

[3] N.A. Vainos, J.A. Khoury, and R.W. Eason, *Opt. Lett.* **13**, 503 (1988).

- [4] J. Khoury *et al.*, *Appl. Opt.* **33**, 8216 (1994).
- [5] N.I. Nazhestkina *et al.*, *Appl. Phys. B: Lasers Opt.* **72**, 767 (2001).
- [6] D. Dirksen and G. von Bally, *J. Opt. Soc. Am. B* **11**, 1858 (1994).
- [7] M.C. Georges and P.C. Lemaire, *Appl. Phys. B: Lasers Opt.* **68**, 1073 (1999).
- [8] A.A. Kamshilin and A.I. Grachev, *Appl. Phys. Lett.* **81**, 2923 (2002).
- [9] V.V. Shepelevich, *Zh. Tekh. Fiz.* **56**, 618 (1986) [*Sov. Phys. Tech. Phys.* **31**, 375 (1986)].
- [10] A. Marrakchi, R.V. Johnson, and J.A.R. Tanguay, *J. Opt. Soc. Am. B* **3**, 321 (1986).
- [11] S. Mallick, D. Rouède, and A.G. Apostolidis, *J. Opt. Soc. Am. B* **4**, 1247 (1987).
- [12] F. Vachss and L. Hesselink, *J. Opt. Soc. Am. A* **4**, 325 (1987).
- [13] G. Pauliat and G. Roosen, *Ferroelectrics* **75**, 281 (1987).
- [14] S. Mallick and D. Rouède, *Appl. Phys. B: Photophys. Laser Chem.* **43**, 239 (1987).
- [15] G. Pauliat, C. Besson, and G. Roosen, *IEEE J. Quantum Electron.* **25**, 1736 (1989).
- [16] E.M. Khramovich and V.V. Shepelevich, *Opt. Spektrosk.* **75**, 1065 (1993) [*Opt. Spectrosc.* **75**, 629 (1993)].
- [17] E.M. Khramovich and V.V. Shepelevich, *Opt. Spektrosk.* **75**, 1289 (1993) [*Opt. Spectrosc.* **75**, 759 (1993)].
- [18] A. Brignon and K.H. Wagner, *Opt. Commun.* **101**, 239 (1993).
- [19] J.R. Goff, *J. Opt. Soc. Am. B* **12**, 99 (1995).
- [20] A.A. Izvanov, A.E. Mandel, N.D. Khatkov, and S.M. Shandarov, *Autom.* **2**, 79 (1986).
- [21] S.I. Stepanov, S.M. Shandarov, and N.D. Khatkov, *Fiz. Tverd. Tela (Leningrad)* **29**, 3054 (1987) [*Sov. Phys. Solid State* **29**, 1754 (1987)].
- [22] S.M. Shandarov, V.V. Shepelevich, and N.D. Khatkov, *Opt. Spektrosk.* **70**, 1068 (1991) [*Opt. Spectrosc.* **70**, 627 (1991)].
- [23] P. Gunter and M. Zgonik, *Opt. Lett.* **16**, 1826 (1991).
- [24] G. Pauliat, P. Mathey, and G. Roosen, *J. Opt. Soc. Am. B* **8**, 1942 (1991).
- [25] V.V. Shepelevich, S.M. Shandarov, and A.E. Mandel, *Ferroelectrics* **110**, 235 (1990).
- [26] V.V. Shepelevich, N.N. Egorov, and V. Shepelevich, *J. Opt. Soc. Am. B* **11**, 1394 (1994).
- [27] E. Shamonina *et al.*, *J. Opt. Soc. Am. B* **15**, 2552 (1998).
- [28] V.V. Shepelevich and P.P. Khomutovskiy, *Pis'ma Zh. Tekh. Fiz.* **24**, 55 (1998) [*Sov. Tech. Phys. Lett.* **24**, 970 (1998)].
- [29] V.V. Shepelevich *et al.*, *Appl. Phys. B: Lasers Opt.* **68**, 923 (1999).
- [30] V.V. Shepelevich *et al.*, *Ferroelectrics* **234**, 289 (1999).
- [31] N.C. Deliolanis, A.G. Apostolidis, E.D. Vanidhis, and D.G. Papazoglou, *Appl. Phys. B: Lasers Opt.* **75**, 67 (2002).
- [32] N. Kukhtarev *et al.*, *Opt. Commun.* **104**, 23 (1993).
- [33] V.V. Shepelevich *et al.*, *Advances in Photorefractive Materials, Effects, and Devices*, OSA TOPS Vol. 27 (Optical Society of America, Washington, D.C., 1999), pp. 353–360.
- [34] D.G. Papazoglou, N.C. Deliolanis, A.G. Apostolidis, and E.D. Vanidhis, *Appl. Phys. B: Lasers Opt.* **71**, 841 (2000).
- [35] S.F. Nichiporko *et al.*, *Pis'ma Zh. Tekh. Fiz.* **26**, 44 (2000) [*Sov. Tech. Phys. Lett.* **26**, 112 (2000)].
- [36] E. Shamonina *et al.*, *Opt. Commun.* **180**, 183 (2000).
- [37] V.V. Shepelevich *et al.*, *Ferroelectrics* **266**, 305 (2002).
- [38] R.V. Litvinov and S.M. Shandarov, *Opt. Spektrosk.* **85**, 1056 (1998) [*Opt. Spectrosc.* **85**, 972 (1998)].
- [39] V.Y. Krasnoperov, R.V. Litvinov, and S.M. Shandarov, *Fiz. Tverd. Tela (St. Petersburg)* **41**, 632 (1999) [*Phys. Solid State* **41**, 568 (1999)].
- [40] R.V. Litvinov and S.M. Shandarov, *Kvant. Elektron.* **31**, 973 (2001) [*Quantum Electron.* **31**, 973 (2001)].
- [41] E.V. Podivilov *et al.*, *Phys. Rev. E* **65**, 046623 (2002).
- [42] E.A. García, I. Casar, and L.F. Magaña, *Opt. Commun.* **204**, 363 (2002).
- [43] H.J. Eichler, Y. Ding, and B. Smandek, *Phys. Rev. A* **52**, 2411 (1995).
- [44] G. Montemezzani and M. Zgonik, *Phys. Rev. E* **55**, 1035 (1997).
- [45] V.V. Shepelevich, *Opt. Spectrosc.* **83**, 161 (1997).
- [46] B.I. Sturman *et al.*, *Phys. Rev. E* **60**, 3332 (1999).
- [47] V.P. Kamenov *et al.*, *Phys. Rev. E* **62**, 2863 (2000).
- [48] S. Mallick, M. Miteva, and L. Nikolova, *J. Opt. Soc. Am. B* **14**, 1179 (1997).
- [49] D.G. Papazoglou, A.G. Apostolidis, and E.D. Vanidhis, *Ferroelectrics* **205**, 87 (1998).
- [50] S.M. Shandarov, *Appl. Phys. A: Solids Surf.* **55**, 91 (1992).
- [51] S.F. Nichiporko, V.V. Shepelevich, N.N. Egorov, and S.M. Shandarov, *Russ. Phys. J.* **44**, 1044 (2001).
- [52] J.F. Nye, *Physical Properties of Crystals* (Oxford University Press, Oxford, 1957).
- [53] K.S. Aleksandrov *et al.*, *Fiz. Tverd. Tela (Leningrad)* **26**, 3603 (1984) [*Sov. Phys. Solid State* **26**, 2167 (1984)].
- [54] D.G. Papazoglou, A.G. Apostolidis, and E.D. Vanidhis, *Synth. Met.* **83**, 281 (1996).
- [55] V.V. Kucha, V.I. Mirgorodskii, S.V. Peshin, and A.T. Sobolev, *Pis'ma Zh. Tekh. Fiz.* **10**, 124 (1984) [*Sov. Tech. Phys. Lett.* **10**, 51 (1984)].
- [56] H.W. Kogelnik, *Bell Syst. Tech. J.* **48**, 2909 (1969).
- [57] M.B. Klein, S.W. McCahon, T.F. Boggess, and G.C. Valley, *J. Opt. Soc. Am. B* **5**, 2467 (1988).
- [58] D.J. Webb and L. Solymar, *Opt. Commun.* **83**, 287 (1991).
- [59] M. Ziari *et al.*, *J. Opt. Soc. Am. B* **9**, 1461 (1992).
- [60] A. Grunnet-Jepsen, I. Aubrecht, and L. Solymar, *J. Opt. Soc. Am. B* **12**, 921 (1995).
- [61] G. Cedilnik *et al.*, *J. Appl. Phys.* **85**, 1317 (1999).
- [62] D. Rouède *et al.*, *Opt. Lett.* **14**, 740 (1989).
- [63] Y. Hu *et al.*, *Opt. Mater. (Amsterdam, Neth.)* **18**, 139 (2001).
- [64] V.V. Shepelevich, N.N. Egorov, P.I. Ropot, and A.A. Firsov, *Kvant. Elektron.* **32**, 87 (2002) [*Quantum Electron.* **32**, 87 (2002)].